Spectra and composition of ultrahigh-energy cosmic rays and the measurement of the proton-air cross section

Paolo Lipari*

Dipartimento di Fisica, Università di Roma, INFN, Sezione Roma "Sapienza", P. Aldo Moro 5, 00185 Roma, Italy

(Received 12 December 2020; accepted 1 April 2021; published 10 May 2021)

The shape of the longitudinal development of the showers generated in the atmosphere by very high-energy cosmic ray particles encodes information about the mass composition of the flux, and about the properties of hadronic interactions that control the shower development. Studies of the shape of the depth of maximum distributions of showers with $E \gtrsim 10^{17.3}$ eV measured by the Pierre Auger Observatory, suggest, on the basis of a comparison with current models, that the composition of the cosmic ray flux undergoes a very important evolution, first becoming lighter and then rapidly heavier. These conclusions, if confirmed, would have profound and very surprising implications for our understanding of the high-energy astrophysical sources. Studies of the shape of the depth of maximum distribution in the same energy range have been used by the Auger and Telescope Array Collaboration to measure the interaction length of protons in air, a quantity that allows to estimate the pp cross sections for values of $\sqrt{s}$ well above the LHC range. In this paper we argue that it is desirable to combine in a self-consistent way the studies of the cosmic ray composition with those aimed at the measurement of the p-air cross section. The latter necessarily provide information on both the fraction of protons in the flux and the properties of the showers generated by protons, that can be of great help in decoding the cosmic ray composition and in constraining the models of air shower development. At the same time a good determination of the cosmic ray composition, in particular of the helium component, is essential to infer correctly from the data the proton-air cross section.

DOI: 10.1103/PhysRevD.103.103009

I. INTRODUCTION

The study of ultrahigh-energy cosmic rays (UHECR) with $E \gtrsim 10^{17}$ eV is essential to develop an understanding of high-energy sources in the universe. At present the shape of the all-particle spectrum in this energy range is reasonably well measured, thanks to the fact that fluorescence light observation [1] of cosmic ray (CR) showers allow a calorimetric, in good approximation model independent measurement of the primary particle energy. The composition of the cosmic ray flux remains, however, more poorly determined. Information about the mass of the primary particle is encoded in the shape of the longitudinal profile of the showers, however the determination of the composition from the data is difficult because the development of the CR showers also depend on the properties of hadronic interactions, that are not well understood. Uncertainties associated with the description of hadronic interactions are the main limitation for the program to determine the CR composition from fluorescence light observations.

It is generally recognized that QCD gives the fundamental Lagrangian that describes hadronic interactions in terms of quark and gluon fields, however at present we are not able to use the theory to compute all phenomenologically relevant quantities from first principles. Experimental studies at accelerators have provided a large amount of information that allows us to model with reasonable accuracy interactions in a broad range of energies, but the study of UHECR requires an extrapolation (up to $\sqrt{s} \simeq 430$ TeV) from the highest energy results (obtained at LHC at $\sqrt{s} = 13$ TeV). This of course also offers the possibility to use CR observations to perform experimental studies of hadronic interactions above the LHC range.

The problem here is that these two goals appear to be in conflict with each other. On one hand, the measurement of the CR composition requires a comparison of the data with models that must include a description of the properties of hadronic interactions, and on the other hand it is problematic to extract information about hadronic interactions from CR data, because the mass composition of the "beam" is not known. An attractive possibility is to use self-consistency in the simultaneous study of several different observables to extract information on both the CR composition and hadronic interactions (see, for example, [2]).

In recent years very large aperture cosmic ray detectors such as the Pierre Auger Observatory in Argentina [3] and the Telescope Array in the USA [4] have collected large statistics of events in the UHE range. Interpretations of the

*paolo.lipari@roma1.infn.it

(higher statistics) Auger observations based on a comparison of the data with Monte Carlo simulations that include detailed descriptions of hadronic interactions suggest that the CR composition is continuously changing with energy [5–8], first becoming lighter (for $E \lesssim 10^{18.3}$ eV) and then very rapidly heavier, with indications that the spectra of different elements have sharp cutoffs at maximum energies that are roughly proportional to the nucleus electric charge Z. These results, if confirmed, would have profound and very surprising implications for high-energy astrophysics, and it is very important to confirm (or falsify) them with additional studies. Studies on the cosmic ray composition have also been performed by the Telescope Array detector [9,10]. The consistency of the Auger and Telescope Array results is under careful study (see the discussions in Refs. [11,12]).

The interpretation of the Auger data in terms of an energy dependent composition is based on a comparison of the data with Monte Carlo models, and the detailed form of the energy dependence of the composition is model dependent. It is therefore very important to try to validate the models used in these studies, and if possible narrow the range of theoretical uncertainties.

The observations of the longitudinal profiles of UHE showers have also been used to obtain measurements of the p-air inelastic (production) cross section [13–17], in an energy range ($\sqrt{s} \simeq 30$–95 TeV for nucleon-nucleon collisions) that is above the maximum energy obtained at LHC. From these measurements it is possible to infer the cross sections for pp collisions using well-established theoretical concepts that relate the properties of hadron-nucleon and hadron-nucleus collisions [18].

These cross section measurements adopt a method pioneered by the Fly's Eye Collaboration [13] that relates the slope of the exponential tail of the distribution of depth of maximum of the showers to the interaction length of protons in air. The authors of these works argue that the results are (in good approximation) model independent, that is insensitive to other properties of hadronic interactions such as the average multiplicity or the inclusive spectra of final state particles, and also insensitive to the exact composition of the CR flux, as long as protons are a significant component.

The main goal of this paper is to argue that there are significant advantages if these two type of studies, that use the same data to achieve different goals (the measurement of the CR mass composition and the p-air cross section) are combined and performed together. The measurement of the proton cross section must after all necessarily identify a proton component, and it is natural to include this information in the study of the CR composition.

A combined study of composition and of the shape of proton-induced showers offers the possibility to reduce the systematic errors for both measurements. In addition, and perhaps even more important, a study where more observables are considered simultaneously allows more stringent tests for the validity of the Monte Carlo codes. It is methodologically important not to discard *a priori* the logical possibility that our current understanding of hadronic interactions is incomplete and that new phenomena, not detectable at lower energy with accelerator experiments, are present in the UHECR range and distort the interpretation of the data. These phenomena can be revealed in multiparameter studies of the shower properties.

This work is organized as follows, in the next section we review some relevant UHECR observations. Section III discusses the evolution of the cosmic ray composition that can be inferred comparing Monte Carlo models with the Auger measurements of the average and width of the depth of maximum of the showers. The following section discusses the measurements of the proton-air cross section obtained from the study of the shape of the $X_{\max}$ distributions, and discusses how this information also allows to estimate the fraction of protons in the cosmic ray flux. The last section contains some final considerations.

II. OBSERVATIONS OF ULTRAHIGH-ENERGY COSMIC RAYS

A. All-particle energy spectrum

Cosmic rays at very high energy can be observed using two different techniques [1]. In the "surface array technique" a network of sensors at the surface of the Earth observes a fraction of the particles in the shower that reach the ground. In the "fluorescence technique" the photons isotropically emitted by nitrogen molecules excited by the passage of a CR shower are observed by telescopes at the ground to reconstruct the longitudinal profile $N(X)$, which is the number of charged particles at column density X.

Integrating the longitudinal profile $N(X)$ over all X and multiplying by the average energy loss $\langle dE/dX \rangle$ of relativistic charged particles in air, one obtains the energy of the shower dissipated as ionization in the atmosphere, a quantity that accounts for most of the primary particle initial energy. Including corrections for the "invisible energy" carried by neutrinos and for the energy dissipated in the ground, the measurement of the longitudinal profile yields then an estimate of the energy of the primary CR particle that is in good approximation independent from its mass, and from the modeling of the shower development. Cosmic ray observatories such as Auger and Telescope Array are hybrid detectors that use both techniques, and the fluorescence light observations can then also be used to calibrate the data of the surface array, allowing a determination of the all-particle spectrum with higher statistics.

Figure 1 show measurements of the all-particle spectrum obtained by the Pierre Auger Observatory (taken from [19] for $E > 2.5 \times 10^{18}$ eV and from [20] at lower energy), and by Telescope Array [21] and TALE [22]. The results are in reasonably good agreement, with some discrepancies

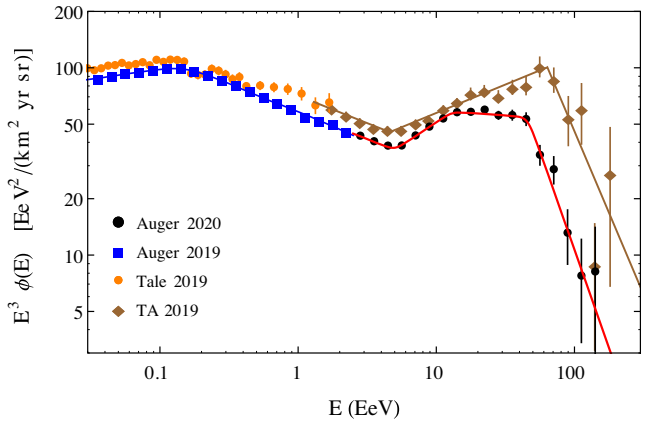

FIG. 1. All particle energy spectrum of very high-energy cosmic rays. The measurements are by Auger [19,20], Telescope Array [21] and TALE [22]. The lines are fits to the data reported in the original publications.

emerging only at the highest energies. The main spectral features are

(A) A softening around $E \simeq 1.5 \times 10^{17}$ eV, commonly called the "second knee."
(B) A marked hardening commonly called the "ankle" observed by both Auger and Telescope Array at $E \simeq 5.0 \times 10^{18}$ eV.
(C) In the energy decade between the second knee and the ankle the all-particle spectrum is well described by a simple power law. The spectral index is estimated by Auger in the entire energy interval [20] as $\gamma_1 = 3.27 \pm 0.05$, and for $E > 2.5 \times 10^{18}$ eV in [19] as $\gamma_1 \simeq 3.29 \pm 0.02 \pm 0.1$. The best fit for Telescope Array [21] is $\gamma_1 \simeq 3.28 \pm 0.02$.
(D) A strong suppression of the flux is observed at $E \approx 5 \times 10^{19}$ eV.
(E) The Auger Collaboration [19,20] has fitted the spectral shape between the ankle and the high-energy suppression as a broken power law, with a spectral break at $E_b \simeq (13 \pm 1 \pm 2) \times 10^{18}$ eV, and exponents $\gamma_2 \simeq 2.51 \pm 0.03 \pm 0.05$ and $\gamma_3 \simeq 3.05 \pm 0.04 \pm 0.10$ in the lower and higher energy range. The spectrum measured by Telescope Array in the same range is consistent with an unbroken power law of slope 2.68 ± 0.02.

To understand the origin of the spectral features in the all-particle spectrum, it seems vital to determine also the composition as a function of energy.

B. Depth of maximum distributions

While the integral of a shower longitudinal profile is entirely determined by the primary particle energy, its *shape* depends on the mass number A of the particle, and on the properties of hadronic interactions. A shower profile can be characterized by several parameters (see, for example, the discussion in [23]), however, essentially all studies until now have relied entirely of the most characteristic one, the depth of maximum $X_{\rm max}$ that is the column density where the profile has its maximum.

Shower development is a stochastic process where fluctuations are large and important. Therefore the showers generated by primary particles of a fixed energy and mass number have a broad distribution of depth of maximum $F_A(X_{\rm max}, E)$. Simulation with Monte Carlo codes allows us to construct predictions for the $X_{\rm max}$ distributions that can then be compared to the data to infer the CR mass composition.

In principle, if one has a good model for the development of the CR showers, it is straightforward to infer the composition of the spectrum from the measurements of the $X_{\rm max}$ distributions. The model allows us to compute the expected shape of the distribution for each particle type, and then one can fit the observed distribution (in each energy bin) using as free parameters the fractions $\{f_A\}$ for different nuclei in the spectrum. This program has been performed by the Auger Collaboration in [5] for showers above an energy of $E = 10^{17.8}$ eV collected from December 2004 to December 2012, interpreting the data using three different Monte Carlo codes. This type of study determines the fractions of all components in the CR flux, including the proton one, and are the best and most complete method to study the composition, avoiding, in principle, the ambiguities of methods that use more limited information such as what is contained in the first two momenta of the distributions.

The discussion on the composition of the CR flux can be simplified (but at the cost of losing some information) studying the first two momenta of the depth of maximum distributions. In the following we will present a study based on this approach, following closely ideas first developed in [24].

Measurements of the average $\langle X_{\rm max} \rangle$ and width $W = \sqrt{\langle X_{\rm max}^2 \rangle - \langle X_{\rm max} \rangle^2}$ of the depth of maximum for the showers detected by Auger [25] in different energy bins are shown in Fig. 2 together with prediction for pure compositions of protons and iron nuclei calculated for three models for shower development: QGSJet II-04 [26], EPOS-LHC [27], and Sibyll 2.3c [28].

Measurements of $\langle X_{\rm max} \rangle$ and W have also been obtained by Telescope Array [29]. The results of the two experiments, however, cannot be directly and easily compared to each other because the measurements made public have not been corrected for significant detector acceptance effects. The question of the consistency between the results on composition of the two experiments has been the object of detailed joint studies [11,12] that will not be reviewed in the present work, which in the following will concentrate on the interpretation of the higher statistics Auger data.

Inspecting Fig. 2 one can see that the three models have predictions for the average and width of the depth of maximum distributions that have some important similarities:

1. The average $X_{\rm max}$ for protons in good approximation grows linearly with $\log E$, with an elongation rate

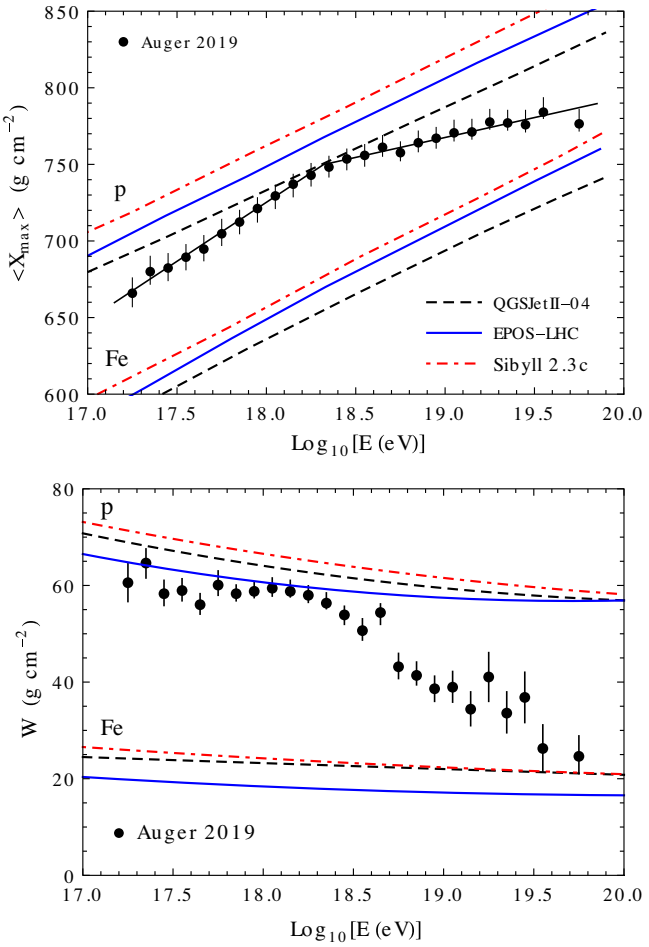

FIG. 2. Measurements of the average $\langle X_{\rm max}\rangle$ (top panel) and dispersion $W = [\langle X^2_{\rm max}\rangle - \langle X_{\rm max}\rangle^2]^{1/2}$ (bottom panel) of the depth of maximum distributions measured by the Pierre Auger Observatory in different energy intervals [25]. The predictions for protons and iron nuclei particles are calculated using the hadronic models QGSJet II-04 [26], EPOS-LHC [27], and Sibyll 2.3c [28].

$D(E) = d\langle X\rangle/d\log E$ that is approximately energy independent. For protons at $E \simeq 10^{18.5}$ the three models have elongation rates that are very similar: 54.0, 56.7, and 57.2 g/(cm^2 decade) (for QGSJet II-04, EPOS-LHC, and Sibyll 2.3c, respectively).

2. The absolute value of the depth of maximum for protons is, however, model dependent, with predictions (always at $E \simeq 10^{18.5}$) for the three models: $\langle X_p\rangle = 760$, 778, and 790 g/cm^2.
3. The average depth of maximum for iron nuclei has approximately the same energy dependence as for protons, so that the difference in $\langle X_{\rm max}\rangle$ between proton and iron showers is approximately constant, and has only a small model dependence, with value $\langle X_p\rangle - \langle X_{\rm Fe}\rangle \simeq 90$–$100$ g/cm^2. This can be understood noting that the shower generated by a nucleus of energy E and mass number A, in good approximation can be described as the superposition of A nucleon showers of energy E/A. The energy and mass dependences of the average depth of maximum can then be summarized with a simple equation that is not exact, but captures the main properties of the current models:

$$\langle X_A(E)\rangle \simeq \langle X_p(E_0)\rangle + D_0 \log\left(\frac{E}{AE_0}\right), \quad (1)$$

where E_0 is an arbitrary reference energy, $\langle X_p(E_0)\rangle$ is the average depth of maximum for protons at this energy, and D_0 is a theoretical "elongation rate" that is approximately energy independent.
4. The width of the $X_{\rm max}$ distributions changes only slowly with energy, and decreases with A, being of order 60 g/cm^2 for protons and 20 g/cm^2 for iron, with only a weak model dependence. First order approximations of the A dependence are $W^2_A \simeq W^2_p A^{-0.5}$, or $W^2_A \simeq W^2_p[1 - a\log A + b(\log A)^2]$ (with a and b adimensional positive constants).

Using the approximation of Eq. (1) one finds that for a mixed composition the average of the depth of maximum distribution at the energy E is

$$\langle X_{\rm max}(E)\rangle \simeq \langle X_p(E)\rangle - D_0\langle \log A(E)\rangle, \quad (2)$$

and depends linearly on the average of the logarithm of the mass number of the particles that form the flux, while the width takes the form

$$W^2(E) \simeq \langle W^2_A(E)\rangle + D^2_0\,\sigma^2_{\log A}(E), \quad (3)$$

where the first term is the average of the widths of the distributions of the different mass components appropriately weighted, and in the second term $\sigma_{\log A}$ is the r.m.s. of the $\log A$ distribution. It is instructive to consider the simple case of a spectrum formed by two components of mass A_1 and A_2, when Eq. (3) can be rewritten (leaving implicit the energy dependence) as

$$W^2 \simeq f_1 W^2_{A_1} + (1-f_1)W^2_{A_2} + D^2_0 f_1(1-f_1)[\log A_1 - \log A_2]^2, \quad (4)$$

where f_1 is the fraction of the flux of the A_1 component. If the two mass numbers A_1 and A_2 are sufficiently different, the last term in the equation, which takes into account the fact that the distributions of the two components are centered on different average values, becomes dominant. For example, combining protons with iron, and using the values for W_p and $W_{\rm Fe}$ of the current Monte Carlo models, one finds that the dispersion of the mixed composition is *larger* than the width for a pure proton composition if $f_p \gtrsim 0.31$, with the broadest distribution ($W \approx 1.15\,W_p$) obtained for $f_p \approx 0.65$. Similarly, combining proton with

silicon, the width of the mixture is broader than for pure protons when $f_p \gtrsim 0.43$, with the broadest distribution ($W \approx 1.08\, W_p$) obtained for $f_p \simeq 0.71$.

In [25] the elongation rate $D_{\rm data}$ of the Auger measurement is fitted to the values 77 ± 2 and 26 ± 2 [in units g/(cm^2 decade)] below and above the energy $E^* \simeq 10^{18.3}$ eV. Since the elongation rate of the models for constant compositions D_0 is predicted to be in the range 54–61 g/(cm^2 decade), one has to conclude that if the models are correct, the CR composition must change with energy, becoming gradually lighter in the lower energy range, and then gradually heavier at higher energy.

The measurements of the width of the $X_{\rm max}$ distribution are a very important constraint on the evolution of the composition. Below $E^* \simeq 10^{18.3}$ eV the width is approximately constant, with a value $W \simeq 60$ g/cm^2 that is consistent with the prediction for a pure proton composition. At higher energy the width decreases monotonically, reaching a value of order 30 g/cm^2 at $E \approx 10^{19.5}$ eV.

The CR composition at a given energy is determined by the set $\{f_A\}$ that give the fractions of the flux in nuclei of mass number A. Given these mass fractions, and a model for shower development that predicts the values of $\langle X_A \rangle$ and W_A, it is straightforward to compute the expected average and width of the depth of maximum distribution. The inverse mapping, however, has not in general a unique solution because different compositions can result in $X_{\rm max}$ distributions that have identical average and dispersion. It has been show [24] that in a reasonably good approximation there is a one to one mapping between $\{\langle X_{\rm max}\rangle, W\}$ and the pair of parameters $\{\langle \log A\rangle, \sigma^2_{\log A}\}$, that give the average and r.m.s. of the $\log A$ distribution.

For any value of the energy, and fixing the model for shower development, there is an allowed region in the plane $\{X_{\rm max}, W\}$, that is a set of values that can be obtained for a possible combination of nuclei. One example of such an allowed region (for $E = 10^{17.5}$ eV and using the QGSJetII-04 model) is shown as a shaded area in Fig. 3. This region has been calculated assuming for simplicity that only five nuclei (p, ^{4}He, ^{14}N, ^{28}Si, and ^{56}Fe) give non-negligible contributions to the CR spectrum. Because of the poor mass resolution of the observations this is a good approximation if one interprets each component as the sum of contributions of the nuclei in appropriate mass number intervals. This description of the composition has been widely used for the study of high-energy cosmic rays.

In the figure one can easily identify the five points that correspond to pure compositions, while the curved lines that connect two such points corresponds to all pairs of values $\{\langle X_{\rm max}\rangle, W\}$ that can be obtained with compositions formed by two components. The boundary of the allowed region is formed by a subset of these two-component lines. The upper part of the boundary is the curve for proton-iron combinations, and the lower part of the boundary is formed

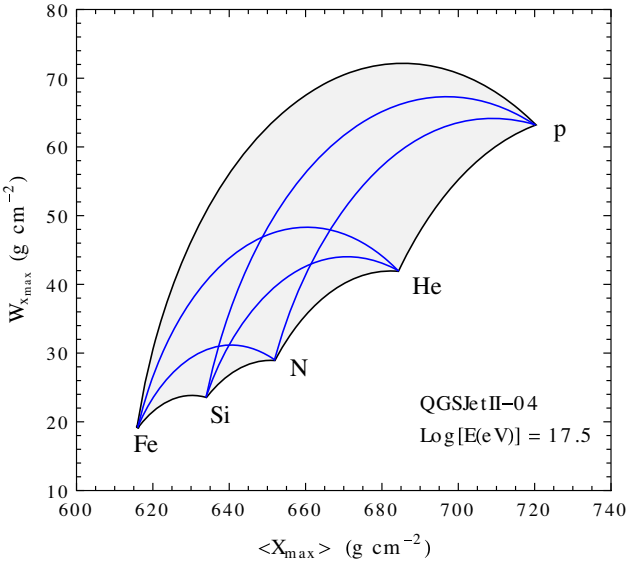

FIG. 3. Allowed region in the plane $\{\langle X_{\rm max}\rangle, W\}$ calculated using the hadronic model QGSJetII-04 [26] at the energy $E = 10^{17.5}$ eV and considering the contributions of 5 nuclei (p, ^{4}He, ^{14}N, ^{28}Si, and ^{56}Fe). The lines show points that can be generated by the combinations of two nuclei.

by combinations of two elements that are adjacent in mass: proton-helium, helium-nitrogen, nitrogen-silicon, and silicon-iron. It should be noted that if the point $\{\langle X_{\rm max}\rangle, W\}$ is near the boundary of the allowed region the composition is a two-component mixture and is uniquely determined.

The allowed region in the plane $\{\langle X_{\rm max}\rangle, W\}$ changes with energy and is determined by the model. This is illustrated in Fig. 4, which shows the allowed region for the three models introduced above and for two values of the primary particle energy ($E = 10^{17.5}$ and $E = 10^{19.5}$ eV). Increasing the energy the allowed region moves to higher values of $\langle X_{\rm max}\rangle$, while the width W changes only slowly.

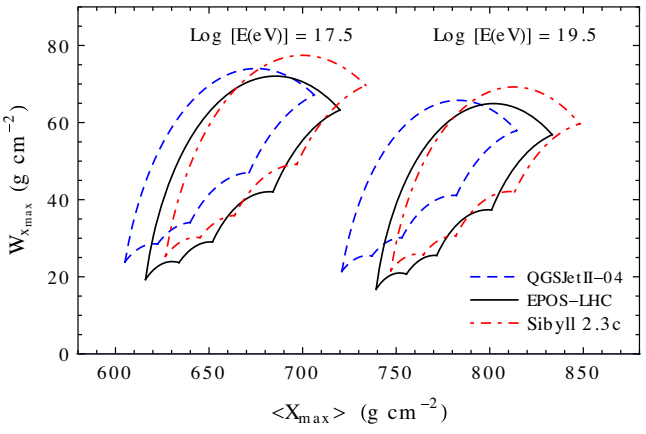

FIG. 4. Allowed regions in the plane $\{\langle X_{\rm max}\rangle, W\}$ calculated using three hadronic models (QGSJetII-04, Epos-LHC, and Sibyll 2.3c) for two energies $E = 10^{17.5}$ and $10^{19.5}$ eV.

From Fig. 4 one can see that the position of the allowed region is energy and model dependent, but has a shape that remains in good approximation constant. This suggests to study the evolution with energy of the CR mass composition introducing rescaled (adimensional) variables:

$$x = \frac{\langle X_{\max}\rangle - \langle X_{\mathrm{Fe}}\rangle}{\langle X_p\rangle - \langle X_{\mathrm{Fe}}\rangle} \tag{5}$$

and

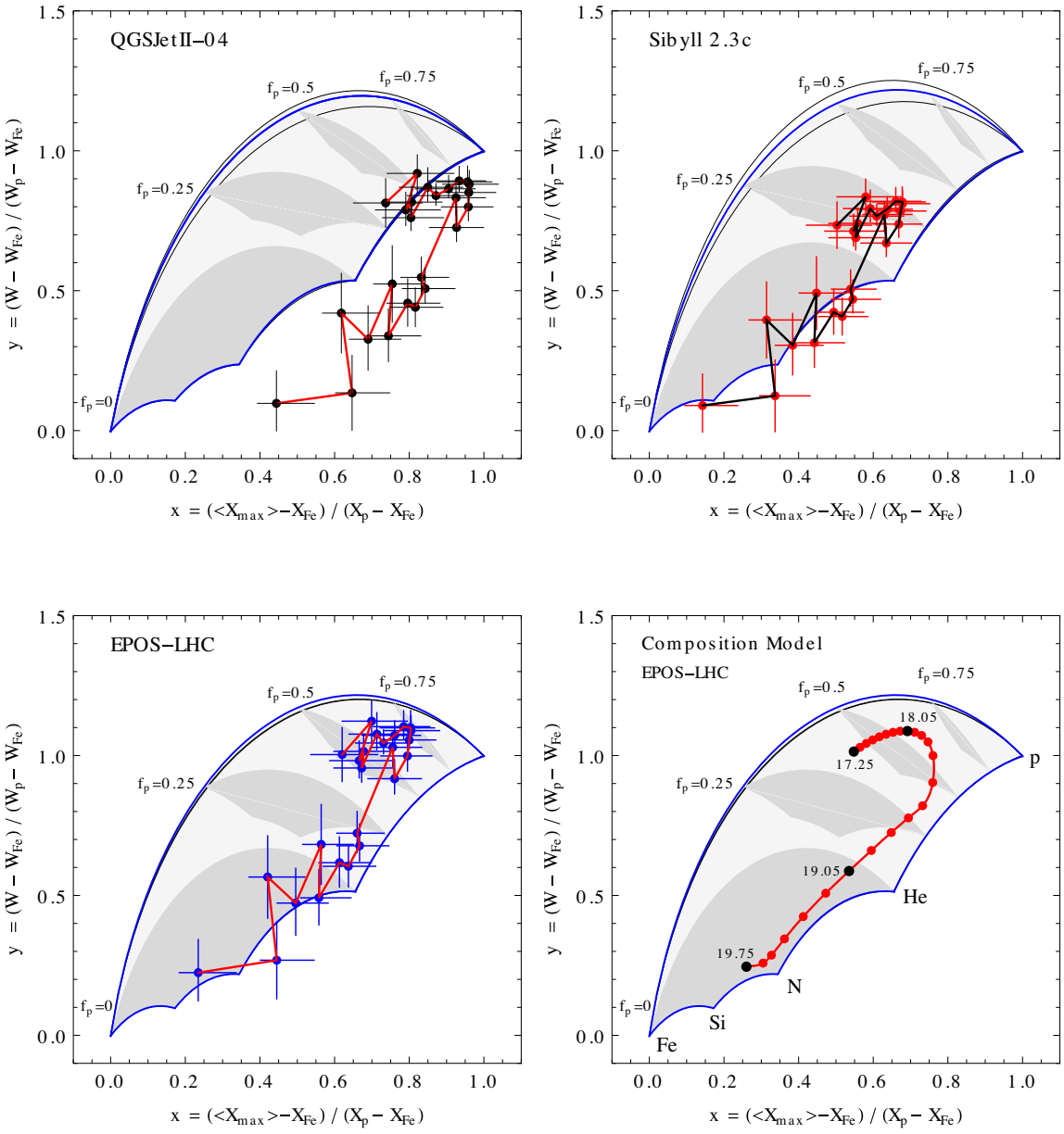

FIG. 5. The Auger measurements of the average and dispersion of the depth of maximum distributions (shown in Fig. 2) are represented as points in the plane of the rescaled variables x and y [see Eqs. (5) and (6)]. Three panels show the results for the three hadronic models QGSJetII-04, Sibyll 2.3c and EPOS-LHC. The contour of the allowed region in the $\{x, y\}$ plane (for each model) has a weak energy dependence, and in each panel the contour is shown for three values of the energy ($\log_{10} E = 17.5$, 18.5 and 19.5), the difference between the contours remains always small. The broken line connects data points in adjacent energy intervals, with the highest energy point the one with the lowest x and y values. The last panel shows the trajectory in the space $\{x, y\}$ for the composition model discussed in the text (and shown in Fig. 8) calculated using the EPOS-LHC model (representative values of $\log[E(\mathrm{ev})]$ are labeled). In all panels the shaded area shows the region of parameters space allowed for the combination of five nuclei considered. The darker shaded areas indicate the parameter regions that are physically possible for a fixed proton fraction [with values $f_p = 0.75$, $f_p = 0.5$, $f_p = 0.25$, and $f_p = 0$ as marked, a pure proton composition ($f_p = 1$) corresponds to the corner at the upper right].

$$y = \frac{W - W_{\mathrm{Fe}}}{W_p - W_{\mathrm{Fe}}}. \quad (6)$$

In these expressions $\langle X_{\mathrm{max}} \rangle$ and W are obtained from the data, while the other quantities must be calculated using a model for shower development.

In good approximation a point in the plane of the rescaled variables $\{x, y\}$ is mapped to the same values of the mass fractions $\{f_A\}$ independently from the energy; therefore the trajectory of the point in this plane that describes the measurements (for different energies) is a good method to visualize the evolution of the CR composition.

This idea is illustrated in Fig. 5 where the Auger measurements of $\langle X_{\mathrm{max}} \rangle$ and W at different energies are shown as points with error bars in the plane $\{x, y\}$ after rescaling the results [with Eqs. (5) and (6)] using the theoretical predictions of the three models (QGSJetII-04, EPOS-LHC, and Sibyll 2.3c).

The first panel in Fig. 5 shows the results for the QGSJetII-04 model. In this case the points at high energy are outside the allowed region indicating that the model is not viable. The second and third panel show the results using the Sibyll 2.3c and EPOS-LHC models. Using these models the Auger observations can have a consistent interpretation, however the evolution of the composition indicated by these studies has some very remarkable and surprising properties, as discussed in the next section.

In Fig. 5 the regions in the plane $\{x, y\}$ plane that correspond to certain representative values of the proton fraction ($f_p = 1$, 0.75, 0.5, 0.25 and 0) are indicated. This allows us to note that at high energy the points that describe the measurements move toward small values of the proton fraction.

III. INTERPRETATION OF THE AUGER DEPTH OF MAXIMUM MEASUREMENTS

In this section we will discuss the interpretation of the fluorescence light observations of Auger. Our discussion will not include an analysis of the observations obtained by the Auger ground array. The ground array data are of great interest and provide very valuable information about the CR composition [30,31], and a combined analysis of all Auger data is not only desirable but necessary, but will not be developed here. It should be noted that the modeling of UHECR showers at ground level, in particular for the muon component, requires a very accurate description of properties of hadronic interactions that do not have a significant role for the longitudinal development (observed by fluorescence light measurements), and is in many ways more difficult. In fact the observations of the muon content of high-energy showers obtained by several detectors have shown anomalies [32–34] that indicate that all existing models have flaws and need to be revised. Understanding the origin of these anomalies remains a very important open problem.

In the following discussion we will assume that the models of hadronic interactions used in the Monte Carlo simulations can correctly predict the shower longitudinal development, and that the anomalies revealed by the observations of muons at ground level are of negligible importance for this type of measurements. This is clearly an assumption that should be critically reanalyzed in future studies.

As discussed above, Auger has measured an elongation rate that is larger than the constant composition prediction below the energy $E^* \approx 10^{18.3}$ eV, and smaller above. This implies that the CR composition is continuously changing, first (for $E < E^*$) becoming gradually lighter and then gradually heavier. Below E^* one also observes that the width of the depth of maximum distribution is approximately constant, while at higher energy it decreases monotonically. These observations also play an important role in determining the evolution of the CR composition.

The energy E^*, where one observes these effects is close (even if not identical) to the energy where the all-particle spectrum exhibits the sharp hardening commonly known as the ankle. This suggests to "identify" E^* and the ankle energy, assuming that the spectral feature and the changes in composition have a common origin. In the following we will first discuss the CR composition at $E \approx E^*$ and then its evolution below and above E^*.

A. Composition for $E \approx E^*$

A good determination of the CR composition around the energy E^*, where it is the lightest, is a crucial element to develop an understanding of very high-energy cosmic rays. Observations of the shape of the tail of the depth of maximum distribution [14] (that we will discuss in more detail below) indicate that around this energy the spectrum contains a large proton component. The estimate of the fraction of the spectrum formed by protons is however model dependent.

Inspecting Fig. 2, one can see that at $E \simeq E^*$ the QGSJet II-04 model predicts for a pure proton composition an X_{max} distribution that (within errors) has the same average and width of the data. This model, however, cannot provide a consistent interpretation of the data because the measurements of $\langle X_{\mathrm{max}} \rangle$ and W at higher energy fall outside the allowed region predicted by the model, as discussed in the previous section. The predictions of the EPOS-LHC and Sibyll 2.3c for the average depth of maximum of a pure proton composition are larger than the Auger measurement, and therefore according to these models the spectrum contains a component of higher mass nuclei.

It is instructive to discuss the case where the spectrum is formed by only two components: protons (that account for a fraction f_p of the spectrum), and nuclei of mass number A (that account for a fraction $1 - f_p$). Using Eq. (2) the

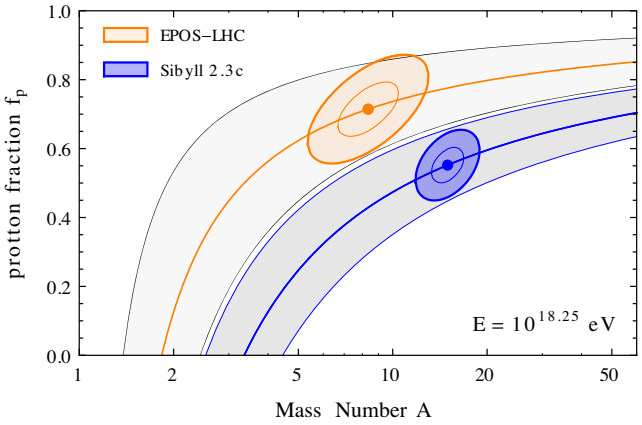

FIG. 6. Interpretation of the Auger measurements $\langle X_{\max}\rangle$ and W at energy $E = 10^{18.25}$ eV in terms of a composition formed by protons and a second component of mass A, using the EPOS-LHC an Sibyll 2.3c models. The thick lines show the proton fraction needed to reproduce the measured value of $\langle X_{\max}\rangle$ as a function of A (with the shaded area a one sigma uncertainty interval). The ellipses show the (one standard deviation) the allowed region in the plane $\{A, f_p\}$ calculated taking into account the measurement of the width W of the depth of maximum distribution.

average and width of the depth of maximum distribution at energy E are

$$\langle X_{\max}\rangle = \langle X_p\rangle - (1 - f_p) D_0 \log A. \tag{7}$$

$$\langle W^2\rangle = f_p W_p^2 + (1 - f_p) W_A^2 + f_p(1 - f_p) D_0^2 (\log A)^2 \tag{8}$$

(where we have left implicit the energy dependence). Using a model for the predictions of the elongation rate D_0, the proton average depth of maximum $\langle X_p\rangle$ and the widths W_p and W_A of the two distributions, Eqs. (7) and (8) allow us to obtain both the proton fraction f_p and the mass number A of the second component from the measurements of $\langle X_{\max}\rangle$ and W.

The results of this exercise at the energy $E = 10^{18.25}$ eV are shown in Fig. 6. For EPOS one finds $f_p \simeq 0.71 \pm 0.09$ and $A \simeq 8^{+4}_{-3}$, and for Sibyll $f_p \simeq 0.55 \pm 0.07$ and $A \simeq 15^{+5}_{-4}$, where the (one σ) errors take into account only uncertainties in the experimental measurements. There is a positive correlation between f_p and A, because one can obtain the same average $\langle X_{\max}\rangle$ with a smaller nuclear component of larger mass number. For both models protons are the most abundant component of the spectrum, but nuclei are not negligible. The fits disfavor compositions where the nuclear component has a very large A, because in this case the predicted width becomes too large (as illustrated in Fig. 7), and the mixing of protons and iron nuclei is not allowed. The proton fraction is smaller in Sibyll, because in this model the showers are more penetrating than in EPOS (by approximately 15 g/cm^2), and therefore a larger contribution from nuclei is required to lower the average depth of maximum and obtain agreement with the data.

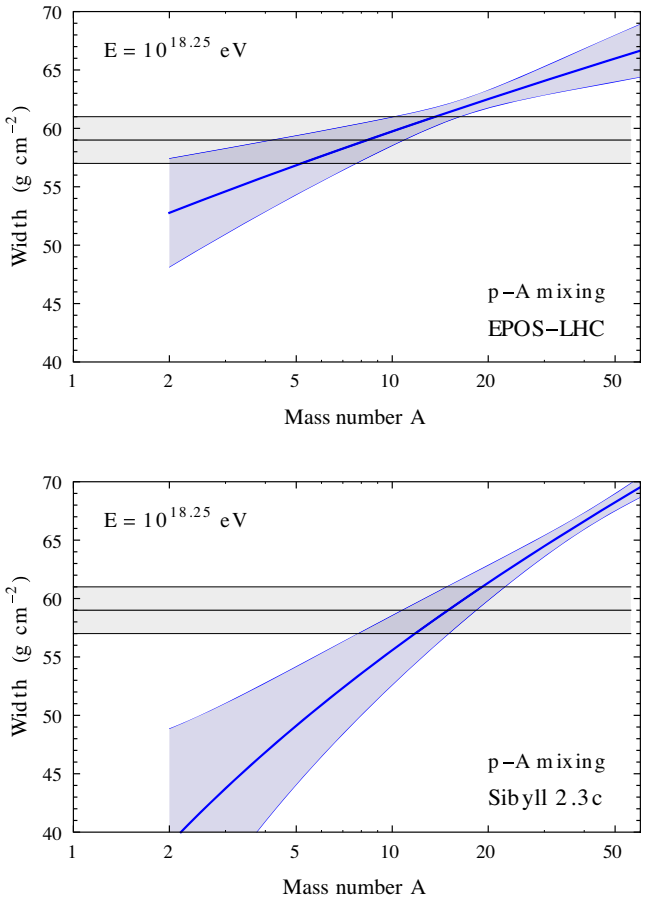

FIG. 7. Width of the depth of maximum distribution predicted at the energy $E = 10^{18.25}$ eV for a composition formed by protons and nuclei of mass number A. For each value of A the proton fraction f_p is determined by the requirement to reproduce the value of $\langle X_{\max}\rangle$ obtained by Auger [25] (the shaded area is a 1σ uncertainty band). The measured value of W (with a 1σ error) is shown as the horizontal band. The top (bottom) panel uses the EPOS-LHC (Sibyll 2.3c) model.

B. Composition below the ankle

The elongation rate measured by Auger in the energy range $10^{17.25}$–$10^{18.25}$ eV has been fitted [25] with a constant value $D_{\text{data}} \simeq 77 \pm 2$ g/(cm^2 decade), that is significantly larger than the model predictions for an energy independent composition that are of order $D_0 \simeq 56$–61 (same units). Using Eq. (2) one finds that the composition is changing with energy with the average $\log A$ that decreases linearly with $\log E$:

$$\frac{d\langle \log A\rangle}{d\log E} \simeq -\left(\frac{D_{\rm data}}{D_0}-1\right) \simeq -0.3 \pm 0.1. \tag{9}$$

The simplest interpretation for this change in composition is to assume that the CR spectrum in this energy range is formed by two components: $\phi_\ell(E)$ and $\phi_h(E)$ one "light" and one "heavy" (with average logarithm of mass number $\log A_\ell$ and $\log A_h$) that have different spectral shapes, with the light component being harder.

Expressing $\langle \log A\rangle$ in terms of the fractions of the two spectral components, and using Eq. (2) for the average $X_{\rm max}$, it is possible to write $f_\ell(E)$ (the light component fraction at the energy E) in the form

$$f_\ell(E) = \frac{1}{\Delta\log A}\left[\log A_h - \frac{\langle X_p(E_0)\rangle - \langle X_{\rm max}(E_0)\rangle}{D_0}\right] + \frac{1}{\Delta\log A}\left(\frac{D_{\rm data}}{D_0}-1\right)\log\frac{E}{E_0} \tag{10}$$

(where E_0 is an arbitrary reference energy and $\Delta\log A = \log A_h - \log A_\ell$). According to this equation the fraction $f_\ell(E)$ grows linearly with $\log E$ with a slope $\propto (\Delta\log A)^{-1}$:

$$\frac{df_\ell}{d\log E} \simeq \left(\frac{D_{\rm data}}{D_0}-1\right)\frac{1}{\Delta\log A} \simeq (0.17\pm 0.06)\,\frac{\log 56}{\Delta\log A}. \tag{11}$$

A larger value of $\Delta\log A$, using Eq. (4), corresponds to a more slow variation of the composition. Note that also the constant term in Eq. (10) has the same dependence on the mass composition of the two components $\propto (\Delta\log A)^{-1}$.

In a two-component model, the fraction $f_\ell(E)$ also determines the width of the $X_{\rm max}$ distribution:

$$W^2(E) = W_p^2 f_\ell(E) + W_A^2[1-f_\ell(E)] + f_\ell(E)[1-f_\ell(E)]D_0^2(\Delta\log A)^2. \tag{12}$$

The data show that in the energy range $10^{17.2}$–$10^{18.3}$ eV the width W is approximately constant with a value of order 60 g/cm^2. This is an important constraint of the possible masses of the two components, that disfavors $\Delta\log A$ too large.

The fraction f_ℓ can only take values in the interval [0, 1], therefore an energy dependence linear in $\log E$ can only be valid in a limited range. It is therefore interesting to discuss a model for the energy dependence of the spectral components that can be extended to a broader range. A simple scenario is one where the two components have both power-law form, and can be written as

$$\phi_{h(\ell)}(E) = \phi^\dagger\left(\frac{E}{E^\dagger}\right)^{-\bar\gamma\mp\Delta\gamma/2}, \tag{13}$$

where $E^\dagger$ is a "crossing energy" where the two components are equal (with value $\phi^\dagger$). In this model the spectral index and the elongation rate (for the all-particle flux) are both energy dependent:

$$\gamma(E) = \bar\gamma - \frac{\Delta\gamma}{2}\tanh\left(\frac{\Delta\gamma}{2}\ln\frac{E}{E^\dagger}\right), \tag{14}$$

$$D(E) = D_0\left[1+\frac{\Delta\ln A\Delta\gamma}{4}\cosh^{-2}\left(\frac{\Delta\gamma}{2}\ln\frac{E}{E^\dagger}\right)\right]. \tag{15}$$

Equation (14) states that the spectral index has value $\bar\gamma \pm \Delta\gamma/2$ for $E \ll E^\dagger$ ($E \gg E^\dagger$), changing gradually around the crossing energy, while Eq. (15) predicts that the elongation rate is equal to D_0 for energies much higher and much lower than $E^\dagger$, and takes a larger value in the intermediate region.

The observations of Auger in the energy range considered [20] are well described by a simple power-law spectrum with exponent $\gamma \simeq 3.27 \pm 0.05$, and a constant elongation rate. The model with two components of power–law form can be made consistent (taking into account measurement errors) with these observations, because for E in an energy interval around the crossing energy $E^\dagger$ determined by the condition

$$\left|\frac{\Delta\gamma}{2}\ln\frac{E}{E^\dagger}\right| \lesssim \frac{1}{2} \tag{16}$$

the arguments of the functions tanh and cosh containing the energy dependence of $\gamma(E)$ and $D(E)$ in Eqs. (14) and (15), are sufficiently small, so that it is possible to substitute $\tanh x \to 0$, $\cosh x \to 1$, so that both quantities can be considered constant with values

$$\gamma \simeq \bar\gamma \tag{17}$$

and

$$D \simeq D_0\left[1+\frac{\Delta\ln A\Delta\gamma}{4}\right]. \tag{18}$$

The last two equations determine the spectral indices of the two components, which have average equal to the slope of the all-particle flux, and difference

$$\Delta\gamma \simeq 4\left(\frac{D_{\rm data}}{D_0}-1\right)\frac{1}{\Delta\ln A} \approx 0.3\,\frac{\log 56}{\Delta\log A}. \tag{19}$$

The difference in spectral index for the two components depends on their masses: $\Delta\gamma \propto (\Delta\log A)^{-1}$, and is large when the mass numbers of the two components are close. A too small $\Delta\log A$ is however not consistent with data because it corresponds [see Eq. (16)] to a too short energy interval where the spectral index and elongation rate can be

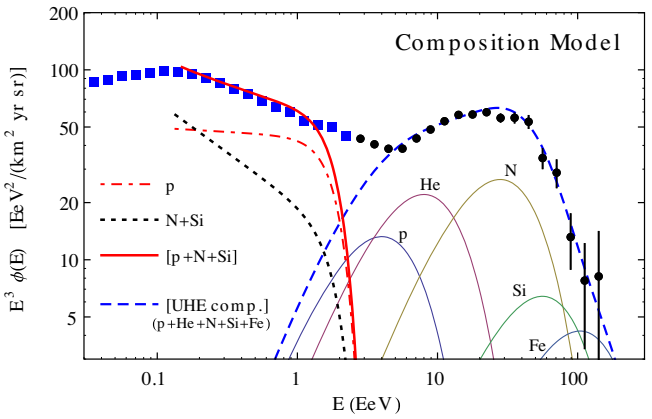

FIG. 8. Model of the CR energy spectrum and composition constructed to reproduce the Auger data. The spectrum below the ankle (shown as a thick solid line) is formed by two component, one of protons and the other of nitrogen and silicon (with equal abundances) that have both power law form with superexponential cutoffs. The spectrum above the ankle (thick dashed line) is formed by the contributions of five nuclei (protons, helium, nitrogen, silicon, and iron) that have a hard power law spectra (with the same slope), with rigidity dependent cutoffs (see main text for more details). The data points are from Auger [19,20].

considered as constant. A too large $\Delta \log A$ is also not viable, because it corresponds to a width W larger than the measurement.

In conclusion, the observations of Auger in the subankle region ($E \lesssim 10^{18.3}$ eV), interpreted with the current models, require a composition that becomes gradually lighter, with an average $\langle \log A \rangle$ that changes by a (modest but significant) 0.3 ± 0.1 in the decade between $10^{17.3}$ to $10^{18.3}$ eV. This change of composition can be described with the mixing of protons with nuclei of intermediate mass (with proton-iron mixing disfavored). A model where the change in composition is due to the combination of two components of power-law form is viable, and results in spectral indices that differ by $\Delta\gamma \approx 0.35$–$0.75$, for compositions with $\Delta \log A \approx 0.7$–$1.4$.

An explicit example of such a two-component scenario, constructed on the basis of the EPOS-LHC model, is shown in Fig. 8. In this model the subankle spectrum is formed by a proton component and a second component of nitrogen and silicon nuclei with equal weight. The average spectral indices of the components $\bar{\gamma} = 3.27$ are equal to the slope of the all-particle flux, the difference in spectral index is $\Delta\gamma = 0.49$, and the crossing energy is $E^{\dagger} = 0.19$ EeV.

C. Composition above the ankle

For $E \gtrsim 10^{18.3}$ eV the elongation rate measured by Auger is significantly smaller than the constant composition predictions, indicating that the composition is rapidly evolving toward a heavier mixture. In this energy range, however, the evolution of the composition cannot be described as the simple combination of two components. This is the consequence of the energy dependence of the width W that decreases rapidly and monotonically from $W \approx 60$ g/cm^2 to ~ 30 g/cm^2.

A qualitative understanding of the evolution of the CR composition can be visualized inspecting Fig. 5 that shows the rescaled measurements of $\langle X_{\rm max} \rangle$ and W for different values of the energy. For the QGSJET model the points that represent the measurements fall outside the allowed region, indicating that the predictions cannot be correct. For the EPOS ans Sibyll model the points are inside the allowed region, but close to the lower boundary. Points on this boundary fully identify the composition, and correspond to the mixing of two elements that are adjacent in mass number.

Using the EPOS-LHC model, for $E \gtrsim 10^{18.5}$ eV, the composition becomes very rich in helium, then evolves to a combination of helium and nitrogen, with the nitrogen fraction that grows with E, and at the highest energy there are indications that silicon begins to mix with nitrogen.

Using the Sibyll 2.3c model, where the showers are on average approximately 15 g/cm^2 deeper, the data are interpreted with a heavier composition, but with an evolution with energy that has the same qualitative features. Above the ankle the composition becomes first a mixture of helium and nitrogen, then of nitrogen and silicon, and finally there is a hint of the appearance of iron at the highest energies.

The very rapid evolution with energy of the composition requires that the spectra of the individual elements are curved, so that they can give a contribution that first increases rapidly, and then rapidly disappears. This requirement can be satisfied in a rather simple model, which has been presented by Auger [7,8] as the most natural framework to interpret the data. In the model the cosmic ray spectra have a rigidity-dependent shape of form:

$$\phi_A(E) \simeq K_A \left(\frac{E}{E_0}\right)^{-\gamma_0} f_{\rm cut}\left(\frac{E}{ZE_{\rm cut}}\right), \tag{20}$$

where A and Z are the mass number and electric charge of the nucleus, and $f_{\rm cut}(x)$ is a cutoff function that is unity for $x \lesssim 1$ and falls rapidly to zero for $x > 1$. The spectra of each element has then a cutoff at an energy that increases linearly with Z. Using this form, the relative contribution of nuclei of charge Z can become dominant in a narrow energy range before its own cutoff, but above the cutoff of nuclei with smaller Z. In this scenario it is then possible to choose the parameters of the spectra so that the all-particle spectrum is dominated by protons for $E \lesssim E_{\rm cut}$, then by helium for $E_{\rm cut} \lesssim E \lesssim 2E_{\rm cut}$, and by more and more massive nuclei as the energy increases.

An example of this scenario is shown in Fig. 8, where the cosmic ray flux above the ankle is fitted as the combination of five nuclei with spectra of the form of Eq. (20) using for the cutoff a simple exponential form: $f_{\rm cut}(x) = e^{-x}$.

The parameters of the fit are $\gamma_0 = 1$, $E_{\rm cut} = 1.8 \times 10^{18}$ eV, and relative mass fractions (for $E \ll E_{\rm cut}$) p:He:N:Si:Fe = 1:0.5:0.05:0.003:0.0004. It should be noted that these parameters describe the CR composition at the Earth. If the CR particles in this energy range are extragalactic, the composition is modified during propagation because of photodisintegration reactions, and a model of the injection is required to infer the composition at the source.

The high-energy component described above accounts for the total of the all-particle flux for energies $E \gtrsim 10^{18.5}$ eV. At lower energy, is contributes only a very small fraction of the total flux, because of its very flat spectrum. On the other hand, the subankle component (modeled as a power law in the discussion above) cannot continue featureless at higher energy, because in this case it would contribute a non-negligible fraction to the total, spoiling the results on composition discussed above. It is therefore necessary to introduce a sharp cutoff for the subankle components (as shown in Fig. 8).

D. The proton fraction

An important result obtained interpreting the Auger results with the current models is the energy dependence of the proton fraction. The form of this energy dependence is illustrated in Fig. 9, using as a model EPOS-LHC. Modeling the CR flux as the combination of two components of protons and nuclei of mass number A, the comparison of the model with the measurement of $\langle X_{\rm max} \rangle$ is sufficient to determine the proton fraction f_p [that can be obtained using Eq. (10) with $A_\ell = 1$]. Curves of $f_p(E)$ obtained in this way for $A = 4$, 14, 28, and 56 are shown in Fig. 9. As already discussed, the measurement of the elongation rate (with a break at $E \simeq 10^{18.3}$ eV), requires that the proton fraction is energy dependent. One can also see that for a smaller mass number A, the proton fraction f_p is smaller and changes more rapidly with energy.

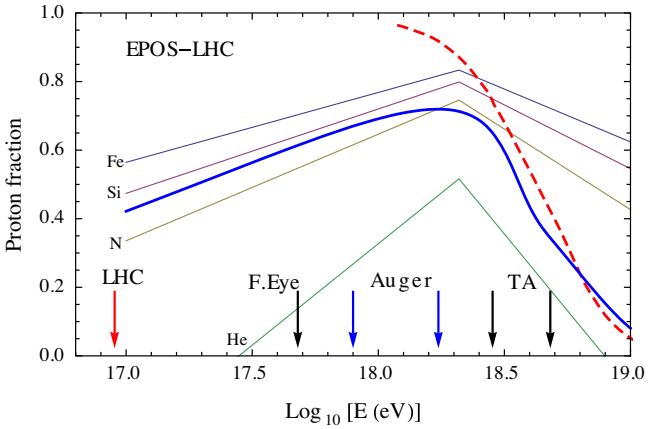

FIG. 9. Fraction of protons in the CR flux as a function of energy. The thin lines are estimates of the proton fraction obtained from the measurements of the average depth of maximum obtained by Auger [25] comparing with the predictions of the EPOS-LHC model and assuming that the composition is formed by the combination of protons and one nuclear component (helium, nitrogen, silicon, and iron) [see Eq. (10)]. The thick solid line is the proton fraction for the model discussed in the text (and shown in Fig. 8). The dashed line is the proton fraction in the very high-energy component discussed by the Auger Collaboration [7,8]. The Auger model does not include the subankle component, but is in good agreement with the superankle component discussed in this paper.

The estimate of the proton fraction requires a model for the mass distribution of cosmic rays at different energies. In this section we have constructed an example of such a model for the composition, where the spectrum is formed by the sum of subankle and superankle components, with the first one formed by two subcomponents (protons and nitrogen plus silicon) of power-law form with a sharp (superexponential cutoff), while the second is formed by subcomponents that have the same hard spectrum with rigidity dependent exponential cutoffs. The proton fraction for this model is shown (as a thick solid line) in Fig. 9. The p fraction grows first (below the ankle) rather slowly, linearly in $\log E$ with a slope 0.47/decade, it reaches a maximum value around $E \simeq 10^{18.3}$ eV, where both components (that at this energy are both rich in protons) give significant contributions, and then (above the ankle) falls very rapidly after the cutoff of the high-energy proton component. The figure also shows (as a dashed line) the proton fraction estimated by Auger [7,8] for the superankle component, which is in reasonably good agreement with the results obtained here. The rapid disappearance of protons at high energy is required in these models to account for the small elongation rate together with the narrowing width of the depth of maximum distribution.

In the bottom part of Fig. 9 the arrows show the energies where different cosmic ray experiments [13–17], using the fluorescence light observations, have obtained measurements of the proton-air cross section. These measurements cover an energy range where, according to the composition studies we have discussed above, the fraction of protons in the CR flux is not constant. It should be noted that all the measurements of the p-air cross section performed by different air-shower detectors have been obtained at different values of the energy, and therefore it is not possible to compare directly the results. It is however surprising that the Auger detector has not presented measurements of the p-air cross section in a broader energy range, since the fluorescence light observations also cover the energy range where Fly's Eye (at lower energy) [13] and Telescope Array (at higher energy) [15,16] detectors have published their measurements. The discussion in [17] suggests that this is due to the fact that at lower and higher energy the proton fraction is smaller, and therefore the measurement of the cross section is more difficult. This however appears to be potentially in conflict with the results presented by the Fly's Eye and Telescope Array detectors. This problem seems

particulary important for the high-energy cross section measurements of Telescope Array, which are obtained in an energy range where the Auger results indicate that the proton component is already significantly suppressed.

These considerations indicate the importance of performing a systematic study of the p-air cross section as a function of energy, together with a measurement of the proton fraction (or more in general of the CR composition).

E. Difficulties for astrophysical models

The evolution of the cosmic ray spectra that emerges from the Auger fluorescence light observations, interpreted with current models for shower development, has some remarkable and unexpected properties, that had not been predicted by any theory, with very important implications for our understanding of the high-energy sources.

1. The spectra of the CR component that dominate at the highest energy, below the cutoff are remarkably hard. The best fit value obtained by the Auger collaboration in [6] is $\gamma_0 = 1.22$; in the present work we have used $\gamma_0 = 1$, which also provides a good description of the data, and that can have some speculative theoretical motivations. This very hard shape is not observed directly, because this component becomes visible only in the energy range where the spectra have sharp cutoffs, however its form can be inferred by the very fast change in the average mass of the CR particles with increasing energy. Such a hard spectral shape is very different to what is observed for cosmic rays at lower energy, and suggests that in this range a new, different acceleration mechanism is operating.
2. A key ingredient of the scenario is the existence of sharp rigidity dependent cutoffs in the spectra. The need for a well-defined cutoff for each component is required by the observation of the very rapid change in mass composition with energy. What is surprising here is not the fact that the cutoffs depend on rigidity, because such dependence is in fact predicted by most acceleration models, but the "sharpness" of these spectral features. It is essentially certain, because of limits on the CR anisotropy, that several sources contribute to the generation of the highest cosmic rays. A well-defined cutoff therefore implies that different sources generate (for each element) spectra with the same maximum energy. This is a very important constraint for the properties (such as geometrical size and magnetic field) of the sources, that calls for an explanation.
3. The shape of the all-particle energy spectrum above the ankle is quite smooth, (even if the Auger Collaboration has recently presented evidence [19] that the energy distribution presents a break and cannot be fitted with a simple power law). The all-particle spectrum is however obtained summing components that all have shapes that are rapidly changing with energy, and the smoothness of the observed spectrum emerges because the relative sizes of the components are sufficiently "fine-tuned." The fit performed here (and by Auger [7,8]) is purely phenomenological, and considers the fraction of different elements in the spectrum as free parameters. This yields a good fit to the all-particle spectrum, but an important question is what the results imply for the mechanism and environment of particle acceleration. In [6] the Auger Collaboration, after modeling the propagation effects, has estimated the mass fractions of the spectra at the source as $f_p : f_{\mathrm{He}} : f_{\mathrm{N}} : f_{\mathrm{Si}} \approx 0.06 : 0.46 : 0.37 : 0.09$ (with a negligible contribution from iron). It is far from easy to construct a realistic astrophysical model to generate this composition of accelerated particles.
4. Below the ankle the all-particle CR spectrum can be described by a simple power-law form with a spectral index of order $\gamma \simeq 3.27$. However, according to the current models, the composition in this energy range is changing, and this requires that the spectra of different elements have different shapes, and the simple power law of the all-particle spectrum emerges only as the sum of these subcomponents. The "standard scenario" where cosmic rays in this energy range are formed by an iron-rich component (perhaps of Galactic origin) and a light extragalactic one do not give a good description of these observations, and one remains with the difficult task to construct a viable astrophysical model.

   The Auger collaboration until now has only discussed a model for the cosmic ray spectra above the ankle. This appears to be a very significant limitation because the study of the composition in the "transition region" where the two components are of similar size, can give very valuable information. A more complete model of the spectra must clearly include a discussion of both the subankle and superankle ranges.
5. A very important result is also the fact that the subankle component is required to have a sharp cutoff around the ankle energy. This is because if this component of the spectrum (that is observed to be rich in protons) continues without a break to higher energy, it would form a large fraction of the all-particle spectrum, in conflict with the results on composition at very high energy. If the subankle spectrum is formed by more than one component, as is suggested by the energy dependence of composition, all important components must have cutoffs, at approximately the same energy. To avoid excessive fine-tuning, this suggests the need to construct a model of CR acceleration where the subankle and superankle components are related. Ideas for such a

common origin have been proposed [35], but the construction of a model that describes the CR spectrum and composition across the ankle remains a very difficult task.

The list of "difficulties" presented above shows how interesting the results obtained by Auger are, that, far from being "disappointing," are in fact quite extraordinary. These considerations suggest however that it is very desirable to perform additional studies that have the potential to give independent support to the validity of the Monte Carlo simulations that play an essential role in the interpretation of the data. An interesting possibility is the study of the proton component, as discussed in the next section.

IV. MEASUREMENT OF PROTON-AIR CROSS SECTION

The shape of the depth of maximum distribution has also been used to measure the proton-air cross section at very high energy. The fundamental idea behind this measurement method was first developed by the Fly's Eye Collaboration [13] and used to obtain an estimate of the cross section for a proton laboratory energy $E \simeq 5 \times 10^{17}$ eV, that corresponds to a c.m. energy for a p-nucleon interaction $\sqrt{s} \simeq 30$ TeV. More recently, estimates of $\sigma_{p\mathrm{Air}}$ have been obtained by the Auger Collaboration at $\sqrt{s} = 57$ TeV [14] and by the Telescope Array Collaboration at $\sqrt{s} = 95^{+5}_{-8}$ [15] and $\sqrt{s} = 73$ TeV [16]. The Auger Collaboration has also presented an estimate of the p cross section at $\sqrt{s} \simeq 48.6$ TeV at the ICRC in 2015 [17].

These papers argue that the measurement of the proton cross section is in good approximation model independent, and is also only weakly dependent on the composition of the cosmic ray flux, as long as the fraction of protons is not too small.

The air shower measurements of the p-air cross section are based on the study of the longitudinal development of the showers. An ideal measurement of the profile would allow us to observe the point X_0 where a primary proton undergoes its first inelastic interaction. The distribution of X_0, for a fixed value of the energy, is a simple exponential:

$$F_0(X_0) = \frac{1}{\lambda_p} e^{-X_0/\lambda_p}, \tag{21}$$

completely determined by the p-air interaction length λ_p, that can be calculated from a combination of the interaction cross sections of protons with the different nuclei that compose the atmosphere:

$$\frac{1}{\lambda_p} = \frac{\sum_A p_A \sigma_{pA}}{\sum p_A m_A} = \frac{\sigma_{p\mathrm{Air}}}{\langle m \rangle} \tag{22}$$

where the summation runs over all nuclei in air, m_A is the mass and p_A the relative abundance for nuclei of type A, and the cross section σ_{pA} is the so-called inelastic production cross section for p-nucleus collisions obtained substracting from the total cross section the elastic and quasielastic (target-fragmentation) contributions, that are essentially invisible in the development of a shower.

The existing detectors do not have the resolution to observe the first interaction point, and therefore cannot simply measure the X_0 distribution and extract λ_p from its shape. The idea introduced by the Fly's Eye Collaboration is that fluctuations in X_0 are the dominant effect in the fluctuations of the depth of maximum $X_{\max}$ for deeply penetrating showers, so that the distribution $F(X_{\max})$ of depth of maximum of the showers takes asymptotically (for large values of $X_{\max}$) the exponential form $F(X_{\max}) \propto e^{-X_{\max}/\Lambda}$ with $\Lambda \approx \lambda_p$. The measurement of this asymptotic shape and of its slope allows then a determination of the p-air interaction length.

To illustrate this point more quantitatively one can note that decomposing the depth of maximum into the sum

$$X_{\max} = X_0 + Y, \tag{23}$$

where X_0 is the position of first interaction point and Y the maximum of the shower development measured from this origin, the $X_{\max}$ distribution can be written as the convolution:

$$\begin{aligned} F(X_{\max}) &= \int_0^\infty dY \int_0^\infty dX_0\, G(Y) \frac{e^{-X_0/\lambda_p}}{\lambda_p} \delta[X_{\max} - (X_0 + Y)] \\ &= \frac{e^{-X_{\max}/\lambda_p}}{\lambda_p} \left[\int_0^{X_{\max}} dY\, G(Y) e^{Y/\lambda_p} \right], \end{aligned} \tag{24}$$

where we have used the fact that the distribution of X_0 is the simple exponential given in Eq. (21) and $G(Y)$ is the distribution of Y, that is determined by the properties of the hadronic interactions and therefore model dependent. Inspecting Eq. (24) one can see that $F(X_{\max})$ converges to the exponential form $\propto e^{-X_{\max}/\lambda_p}$ if the factor in square parenthesis in the right-hand side of the last equation becomes constant for large values of $X_{\max}$. This is true if the function $G(Y)$ vanishes sufficiently rapidly for large Y, so that replacing with infinity the upper limit of the integration does not change the result.

This conclusion can be also obtained studying the $X_{\max}$ dependent slope $\Lambda(X_{\max})$. Dropping the subscript in the notation for $X_{\max}$ one has:

$$\begin{aligned} \frac{1}{\Lambda(X)} &= -\frac{1}{F(X)} \frac{dF}{dX} = \frac{1}{\lambda_p} - \frac{1}{\lambda_p} \frac{G(X)}{F(X)} \\ &= \frac{1}{\lambda_p} - \frac{G(X)}{\int_0^X dY G(Y) e^{(Y-X)/\lambda_p}}. \end{aligned} \tag{25}$$

For large X the slope Λ converges to λ_p if, in the limit $X \to \infty$, the last term in the equation vanishes. This is the

case if the product $G(Y)e^{Y/\lambda_p}$ does not diverge too rapidly for $Y \to \infty$, a condition that it satisfied in essentially all models for shower development (see more discussion and one example below).

Equation (25) has the interesting implication $1/\Lambda(X) < 1/\lambda_p$, and therefore

$$\Lambda(X) > \lambda_p. \tag{26}$$

This inequality follows from the fact that the correction term in Eq. (25) is always negative because the functions F and G are both probability densities and can only have positive values, and states that the depth of maximum distribution of a pure proton composition can never fall more steeply than the asymptotic exponential behavior for large $X_{\max}$. A "flattening" of the distribution is however possible for a composition that includes nuclei, and the value of $X_{\max}$ where the flattening occurs would identify the transition from a range of $X_{\max}$ where nuclei give the largest contribution, to a range where protons are dominant.

In this discussion the quantity $\Lambda(X)$ is a differential slope that changes continuously with the depth of maximum, reaching asymptotically (from above) the value λ_p. In practice the experimental studies for the measurement the p-air interaction length have fitted the tail of the depth of maximum distribution above a minimum value with simple exponential form. The slope Λ of the fit is then related to the p-air interaction length using an adimensional correction factor K:

$$\Lambda = K\lambda_p. \tag{27}$$

The correction factor K depends on the range where the fit is performed, and is always $K > 1$ because of the inequality (26), decreasing toward unity when the fit is performed for larger $X_{\max}$ values. The factor is also model dependent, because the exact form of the convergence of the slope to λ_p is determined by the details of shower development, encoded in the function $G(Y)$.

The method outlined above to measure the p-air cross section can also be used when the CR flux is formed not only by protons, but also include nuclei. This is because protons are the most penetrating of the CR components, and therefore selecting showers with larger and larger $X_{\max}$ one also selects a sample of events where protons give a larger and larger contribution to the distribution. In the practice of course, this program is possible only if protons are a sufficiently large fraction of the CR spectrum.

A. Monte Carlo calculations

To study in more detail the problem of extracting the p-air cross section from cosmic ray observations we have performed some Monte Carlo simulations, calculating numerically the longitudinal development of showers generated by very high-energy cosmic particles. For each simulated shower it is then possible to find the position of the depth of maximum, obtaining $X_{\max}$ distributions with large statistics. The simulations were performed for four types of primary particles (protons, ^{4}He, ^{16}O, and ^{56}Fe) at $E = 10^{18.25}$ eV (approximately the same energy for which Auger [14] has published its measurement of the p-air cross section). The shower development was modeled using the Sibyll 2.1 code [36] to generate the final state of the hadronic interactions, however, the interaction lengths for protons and nuclei adopted to propagate particles in air were recalculated using Glauber theory [18] and starting from phenomenological fits to the total and elastic pp cross sections (shown in Fig. 10) that are in good agreement eith the recent measurements at high energy performed at LHC [37–39].

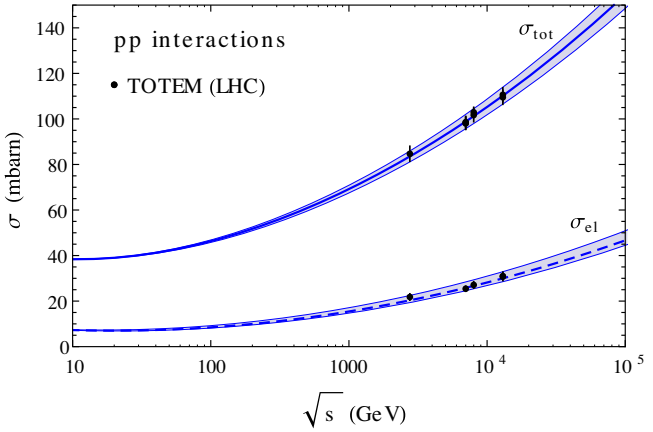

FIG. 10. Total and elastic pp cross sections plotted as a function of the c.m. energy $\sqrt{s}$. The points are measurements of the TOTEM detector at the LHC [37–39]. The solid lines are fits to the total and elastic cross sections that are quadratic in log s [39]. The shaded areas are estimates of the uncertainties.

The resulting p-air interaction length is shown in Fig. 11 together with an uncertainty band (the shaded area) obtained combining the uncertainties for $\sigma_{pp}^{\rm tot}$ and $\sigma_{pp}^{\rm el}$ shown in Fig. 10. The uncertainty estimated in this way is rather small, of order $\approx \pm 3$ g/cm^{-2} for the interaction length, or ± 30 mbarn (± 40 mbarn) for $E \simeq 10^{18}$ eV ($E \simeq 10^{20}$ eV) for the p-air cross section. It must of course be stressed that this is based on an extrapolation. In the following, we will refer to this model that combines Sibyll 2.1 with the modified interaction lengths as Sibyll 2.1a.

The depth of maximum distributions for the four nuclei are shown in Fig. 12. The averages, widths, and also the slopes of exponential fits to the tails of these distributions are shown in Fig. 13. Inspecting these results one can observe the following features.

1. Showers generated by more massive nuclei are less penetrating, and the average $\langle X_{\max} \rangle$ (top panel of Fig. 13) is in good approximation linear in log A in agreement with expectations [see Eq. (1)].

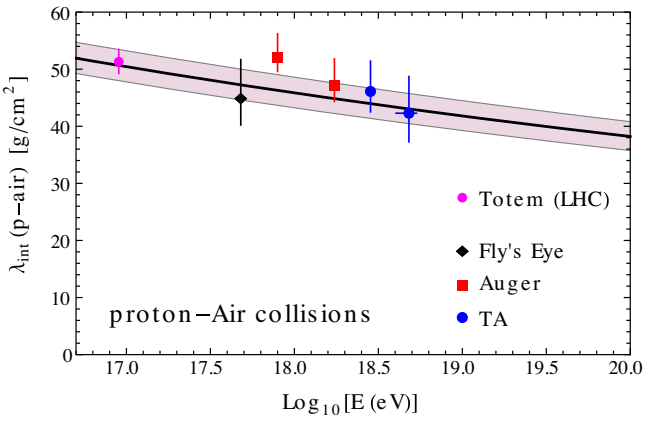

FIG. 11. Proton interaction length in air plotted as a function of the projectile laboratory energy. The central line and the shaded area are calculated using the best fits to the total and elastic pp cross sections and the uncertainties shown in Fig. 10, and using the algorithms of Glauber and Matthiae [18] to estimate the proton-nucleus cross sections. The points are the estimates of the proton-air interaction length obtained from measurements of the longitudinal developments of cosmic ray showers by Fly's Eye [13], Auger [14], and Telescope Array [15,16]. The lowest energy point is calculated from the measurements at $\sqrt{s} = 13$ TeV by TOTEM at LHC [39].

2. The width of the distributions becomes narrower for larger A. This is illustrated in the central panel of Fig. 13.
3. For large values of $X_{\max}$ the distributions are reasonably well described by simple exponentials

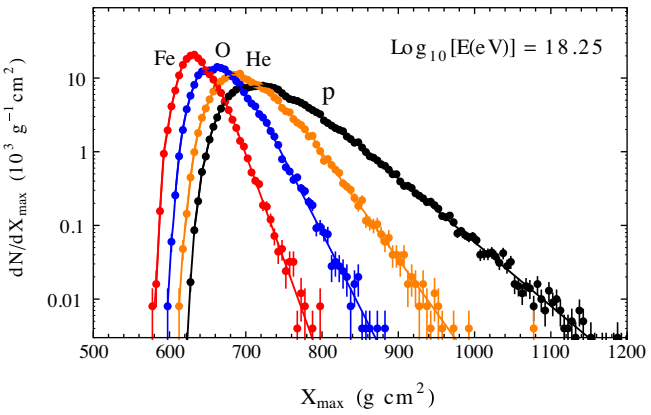

FIG. 12. Distributions of $X_{\max}$ for showers generated by particles with energy $E = 10^{18.25}$ eV. The distributions are calculated with Monte Carlo methods using the Sibyll 2.1 model and the p-air interaction length shown in Fig. 11, for four different nuclei: protons, ^{4}He, ^{16}O, and ^{56}Fe. The high $X_{\max}$ part of the distributions has been fitted with a simple exponential form: $dN/dX_{\max} \propto e^{-X_{\max}/\Lambda}$.

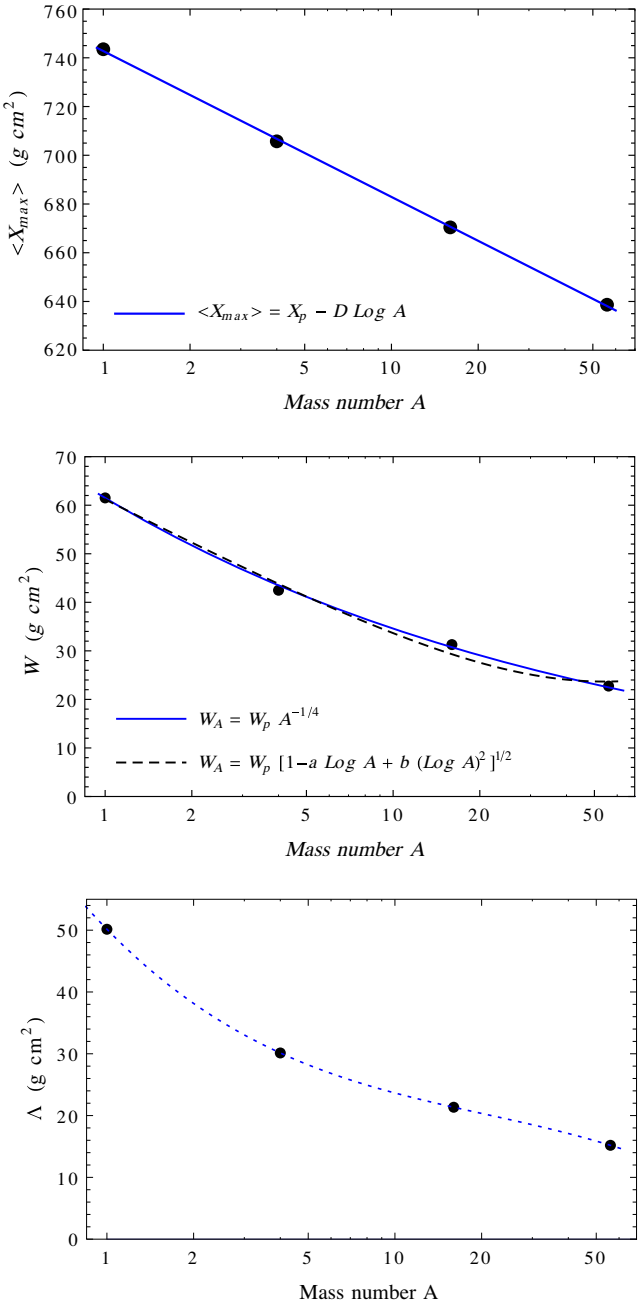

FIG. 13. Parameters of the distributions of $X_{\max}$ for the showers four different nuclei (protons, helium, oxygen, and iron) at energy $E = 10^{18.25}$ eV shown in Fig. 12. The top panel shows the average $\langle X_{\max}\rangle$, and the line is a linear fit for the relation $\langle X_{\max}\rangle = X_0 + D \log A$. The middle panels shows the r.m.s. of the distributions $W = \sqrt{\langle X^2_{\max}\rangle - \langle X_{\max}\rangle^2}$, and the two lines are analytical approximations of the A dependence ($W_A = W_p A^{-0.25}$ and $W_A = W_p[1 - a\log A + b(\log A)^2]^{1/2}$). The bottom panel shows the parameter Λ that fits the high-energy part of the distributions. The line is a polynomial fit to the $\log A$ dependence.

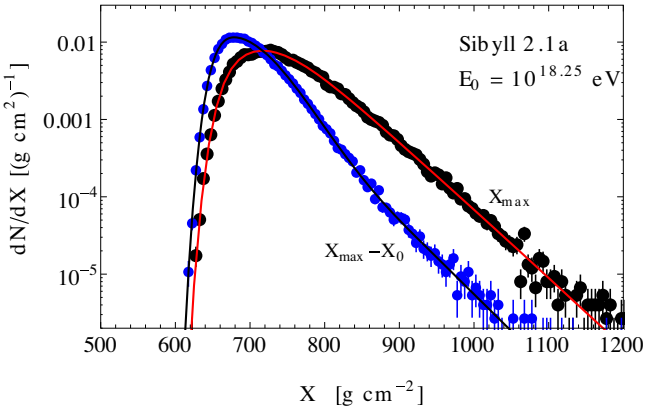

FIG. 14. Distribution of $X_{\max}$ (bigger points) and $Y = X_{\max} - X_0$ (smaller points) calculated for proton showers with energy $E_0 = 10^{18.25}$ eV using the Sibyll code and a shower Monte Carlo model. The thin (black) line is a fit to the Y distribution described in the main text. The thick (red) line is obtained convoluting the previous result with an exponential with slope equal to the interaction length $\lambda_p(E_0)$.

$F_A(X) \propto e^{-X/\Lambda}$, with a slope that depends on the mass number A. The lines in the figure have (for $A = 1$, 4, 16, and 56) slopes $\Lambda = 50.1$, 30.1, 21.3, and 15.2 g/cm^2.

As discussed above the shape of the tail of the $X_{\max}$ distribution for protons is related to the proton-air interaction length, that in this calculation has the value $\lambda_p = 45.9$ g/cm^2. In a Monte Carlo calculation the position of the first interaction point for each simulated shower is known, and therefore it is possible to study the distribution of the quantity $Y = X_{\max} - X_0$ (that is the depth of maximum measured from the point of first interaction), and test the validity of Eqs. (24) and (25).

The distributions of Y and $X_{\max}$ for the proton showers are shown in Fig. 14. The Y distribution has been fitted with a smooth curve. The convolution of this curve with an exponential of slope λ_p [see Eq. (24)] yields a curve (shown as a red line in the figure) that is a very good description of the $X_{\max}$ distribution. From this expression it is possible to compute the $X_{\max}$ dependent slope $\Lambda(X_{\max})$, that is shown in Fig. 15, where one can see that the slope approaches from above, in agreement with Eq. (26), the value λ_p (also shown in the figure as a dashed line). The convergence of $\Lambda(X_{\max}) \to \lambda_p$ is quite slow due to the fact that the distribution of $G(Y)$ has also an exponential form for large values, with a slope that is also approximately equal to λ_p. This can be understood noting that the tail of the Y distribution is formed by events where the final state of the first interactions contains a "leading nucleon" that carries a large fraction of the initial energy and will then form most of the shower. Because of this slow convergence, the shape of the tail can in practice be well fitted with a constant slope in agreement with the "K-factor method" introduced by the Fly's Eye Collaboration [13]. This factor is model dependent, because it encodes the details of shower development, but it also depends on the $X_{\max}$ range where the exponential fit is performed. This range must be chosen finding a compromise between the need to have a sufficiently high statistics (a large range), and the desire to have a correction factor closer to unity (a small range).

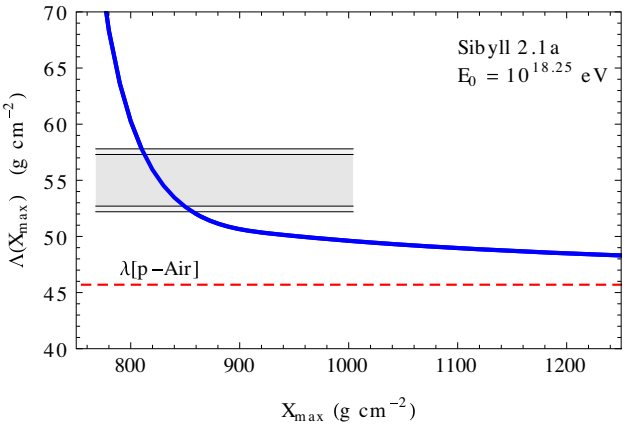

FIG. 15. Slope $\Lambda(X_{\max})$ of the $X_{\max}$ distribution obtained with a Monte Carlo calculation for protons of energy $E_0 = 10^{18.25}$ eV and shown in Fig. 14. The dashed line shows the p-air interaction length used in the Monte Carlo calculation. The shaded area shows the range of $X_{\max}$ and the best fit value for Λ in the study of Auger in [14].

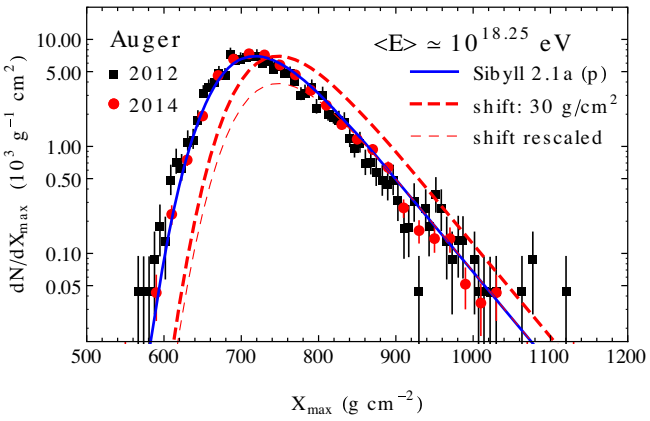

FIG. 16. The points show the depth of maximum distribution observed by Auger for showers with a reconstructed average energy around $10^{18.25}$ eV [14] and [40,41]. The thick solid line is the prediction of the Sibyll 2.1a (that is the model in [36] with the interaction lengths discussed in the main text) for a pure proton composition. The thick dashed line is the same distribution with the showers deeper by 30 g/cm^2 (the difference in average depth of maximum between showers simulated with the Sibyll 2.1 and Sibyll 2.3c models). In this case the proton fraction is of order $f_p \simeq 0.55$.

B. Comparison with the Auger observations

In Fig. 16 we compare the $X_{\max}$ distribution for protons simulated with Sibyll 2.1a with the Auger observations after smearing the distribution with a Gaussian resolution with a width of 25 g/cm^2. The Auger data are taken from two sources. One set of data points is obtained from figure 1 in [14], the work that discusses the measurement of the p-air cross section, and refers to showers observed from December 2004 to September 2010 in the energy range between $10^{18.0}$ and $10^{18.5}$ eV, selected to reduce distortions due to detection acceptance effects. The second set of points are taken from data tables publically available online [40,41], and refer to showers observed from December 2004 to September 2012 in the energy range $10^{18.2}$–$10^{18.3}$ eV.

The comparison of data and simulation is consistent with the conclusions of the Auger collaboration [14] that obtains for the p-air cross section the value $\sigma_{p\mathrm{Air}} = 505 \pm 22^{+28}_{-36}$ mbarn, that corresponds to the interaction length $\lambda_p = 47.9 \pm 2.1^{+3.7}_{-2.5}$ g/cm^2. This result has been obtained fitting the $X_{\max}$ distribution in the interval between 768 and 1004 g/cm^2 with an exponential shape, with a best fit slope $\Lambda = 55.8 \pm 2.3 \pm 1.6$ g/cm^2 (where the two errors are statistical and systematic), and then estimating a correction factor using Monte Carlo calculations.

In our simulation the p-air interaction length is set to the value 45.9 g/cm^2, and the shape of the tail of the $X_{\max}$ distribution is consistent with what is observed by Auger. In Fig. 15 the (X dependent) slope of the simulation (calculated with good precision using 10^5 events) is shown together with the Auger result, showing reasonably good agreement.

The main goal of the comparison of the simulation with the data is not to rediscuss the estimate of the p-air cross section obtained by Auger, but to argue that it is possible to use the study of the tail of the $X_{\max}$ distribution to obtain information about the proton fraction in the cosmic ray spectrum. These results can then be used to constrain the models for shower development.

The measurement of the p-air cross section in fluorescence light detectors is based on the study of the *shape* of the *tail* of the $X_{\max}$ distribution, that is fitted with an exponential. In the cross section study the slope Λ of the fit is related to the interaction length λ_p, but the normalization is discarded [where the normalization is the factor F_0 in the exponential fit $F(X_{\max}) = F_0 e^{-X_{\max}/\Lambda}$, with the distribution $F(X_{\max})$ normalized to unity for integration over all values of $X_{\max}$]. Also the shape of the $X_{\max}$ distribution in the range where it is not of exponential form is not analyzed. There are however some obvious merits in studying not only the shape of the exponential tail of the distribution, but also its normalization, that accounts for the fraction of events that form it, and in comparing data and models in the entire $X_{\max}$ range.

The interest of such a comparison can be illustrated inspecting Fig. 16. In this figure the data and the Monte Carlo distributions are both plotted normalized to unity, and one can see that the exponential tails of the two distributions agree (within errors) both in shape and in normalization, and in fact that the agreement is reasonably good for all values of $X_{\max}$. If we make the assumption that the distribution of the data is not distorted by significant detection acceptance biases, this agreement between data and simulation indicates that the Sibyll 2.1a model can provide a consistent description of the Auger observations at the energy considered ($E \approx 10^{18.25}$ eV) if the cosmic ray spectrum has a pure proton composition. The same conclusion can also be reached comparing the values of $\langle X_{\max} \rangle$ and W of the data and of the Monte Carlo distribution (for a pure proton composition), however the good matching of the shape of the distribution adds valuable information.

The result on composition is of course model dependent. A more recent version of the Sibyll code (Sibyll 2.3c [28], used for comparison in the Auger analysis discussed above) predicts that proton showers are on average approximately 30 g/cm^2 deeper, with a distribution of approximately the same shape and width. For a first order discussion in Fig. 16 the Sibyll 2.3c model is represented shifting by 30 g/cm^2 the distribution of the older version. The tail of the $X_{\max}$ distribution of a proton spectrum simulated with the Sibyll 2.3c model has in good approximation the same slope, but (since the showers are more penetrating), a higher normalization. It is then possible to match the proton simulation to the Auger data, but this requires to reduce the proton fraction by a factor of nearly 2 (the best fit value is $f_p \approx 0.55$). The renormalized proton distribution is shown in Fig. 16 as a thin dashed line, and one can immediately see that this requires the addition of more massive nuclei to the spectrum because the proton component cannot account for the showers that have small $X_{\max}$.

More in general, the slope of the exponential tail of the $X_{\max}$ distribution does offer (if protons are dominant in this range) a measurement of the p-air cross section, that is in good approximation model independent, but then the matching of the normalizations of the data and of the proton simulation in the range where the two distributions have an exponential shape allows us to obtain a (model dependent) estimate of the proton fraction.

Note that the proton fraction cannot be larger than unity, and therefore the study of the normalization outlined above can exclude models where the showers are not sufficiently penetrating. In fact from the results shown above one can conclude that models of shower development where the average depth of maximum is smaller than the Sibyll 2.1a predictions are strongly disfavored by the observations.

It is natural and in fact very desirable to combine the determination of the proton fraction obtained from the study of the most penetrating showers with a composition

study that fits the global shape of the depth of maximum distribution.

It might appear that the two programs of (i) using the observations of the depth of maximum distribution for measuring the proton cross section and/or (ii) use knowledge or theoretical assumptions about the cross section to measure a (model dependent) proton fraction, are mutually exclusive. But this is not the case, and it is in fact possible to perform these studies simultaneously. The point is that we have a very robust prediction that the $X_{\max}$ distributions of protons and helium (the lightest nucleus that can contribute significantly to the CR spectrum) have tails of very different shape, with slopes that differ by a factor ($\gtrsim$1.5) sufficiently large to allow the identification of a proton component (or a setting of an upper limit to the proton fraction) with a reasonably good confidence level. A slope in the range 45–60 g/cm^2 can be safely associated to the existence of a proton component, and used (including an appropriate and weakly model dependent correction factor) to estimate the p-air interaction length. At the same time the normalization of the distribution in the range where the exponential form is valid can be interpreted as a (more strongly model dependent) estimate of the proton fraction.

The shape of the depth of maximum distribution below the range where it has an exponential form encodes other properties (beyond the total inelastic cross section) of hadronic interactions that are relevant to the development of proton showers, and the contributions of nonproton components in the CR flux. To extract as much information as possible from the data, constraining the shower models, and determining the CR composition, it can be important to have a precise fit of the distribution in its exponential range. Vice versa, to avoid biases in performing the fit of the tail of the distribution, knowledge of the composition is necessary. These considerations suggest performing combined studies of the CR composition studies and of the p-air cross section.

A question that emerges naturally is when the proton fraction is sufficiently large to allow a measurement of the p-air cross section. The answer clearly depends on the statistics obtained by a detector, because the measurement (for a fixed energy) requires a sufficiently large number of proton showers in the range where the $X_{\max}$ distribution can be (at least in reasonably good approximation) described by an exponential. The fraction of proton events with depth of maximum in this range is model dependent. The Monte Carlo codes discussed in this paper [26–28,36] indicate that, for a pure proton composition, the exponential tail of the depth of maximum distribution contains a fraction of order 0.2 of all events, with only a weak energy dependence (with different models having the tail in different $X_{\max}$ intervals). This result, which is consistent with the observations if one assumes that the composition is dominated by protons, implies that a dataset of 500 proton showers allows a cross section measurement with a statistical error of order 10%.

If the proton fraction is $f_p \gtrsim 0.1$ and the nuclear component is made of carbon or heavier nuclei, then the contamination in the relevant tail of the proton distribution is expected to be negligible; in other cases the measurement requires the selection of a smaller fraction of (more deeply penetrating) proton showers, or the calculation of a large (and model dependent) correction factor. The possible existence of a helium contamination is in fact a very important source of systematic error. A helium contribution can make the observed depth of maximum distribution steeper (in the range of interest) and this, if no correction is applied, would result in an overestimate of the cross section. For example, in [14] the Auger Collaboration gives a central value of the proton cross section assuming a negligible helium fraction and estimates a systematic error of -30 mbarn for a maximum helium contamination of 25%. Similar considerations for the estimate of the systematic error are also discussed by the Telescope Array collaboration in Refs. [15,16].

The helium contamination can be reduced limiting the analysis to a smaller fraction of events. For example for a spectrum with equal contributions of protons and ^{4}He, the simulations suggest that the helium contribution can be kept smaller than 10% fitting only a fraction $\eta \lesssim 0.05$ of all events. The best strategy for the measurement of the cross section is therefore to find a balance between the isolation of a smaller but more pure proton component, and the study of a larger sample of data with the inclusion of a correction constructed on the basis of a composition study.

C. Energy dependence of the proton fraction

The measurements of the p-air cross section obtained from fluorescence light observations [13–17] span, in terms of laboratory energy, a range (from $10^{17.68}$ eV to $10^{18.68}$ eV) where there are indications that the CR composition undergoes a significant evolution (see Fig. 9), and where the determination of the composition is strongly model dependent. A program to study systematically, as a function of energy, the shape of the tail of the $X_{\max}$ distribution with the goal of estimating simultaneously the p-air cross section and the proton fraction could then not only determine more accurately the p-air cross section, but also give very valuable information on the energy dependence of CR composition, and so constraining hadronic models.

This study requires taking into account detector acceptance effects that can generate significant distortions in the experimental distributions, and cannot be performed here; however, for a very preliminary exploration of the potential of such a program we have analyzed some publically available data of the Pierre Auger Observatory for showers with energy larger than $10^{17.8}$ eV collected from December 2004 to December 2012 [40,41]. One example of $X_{\max}$

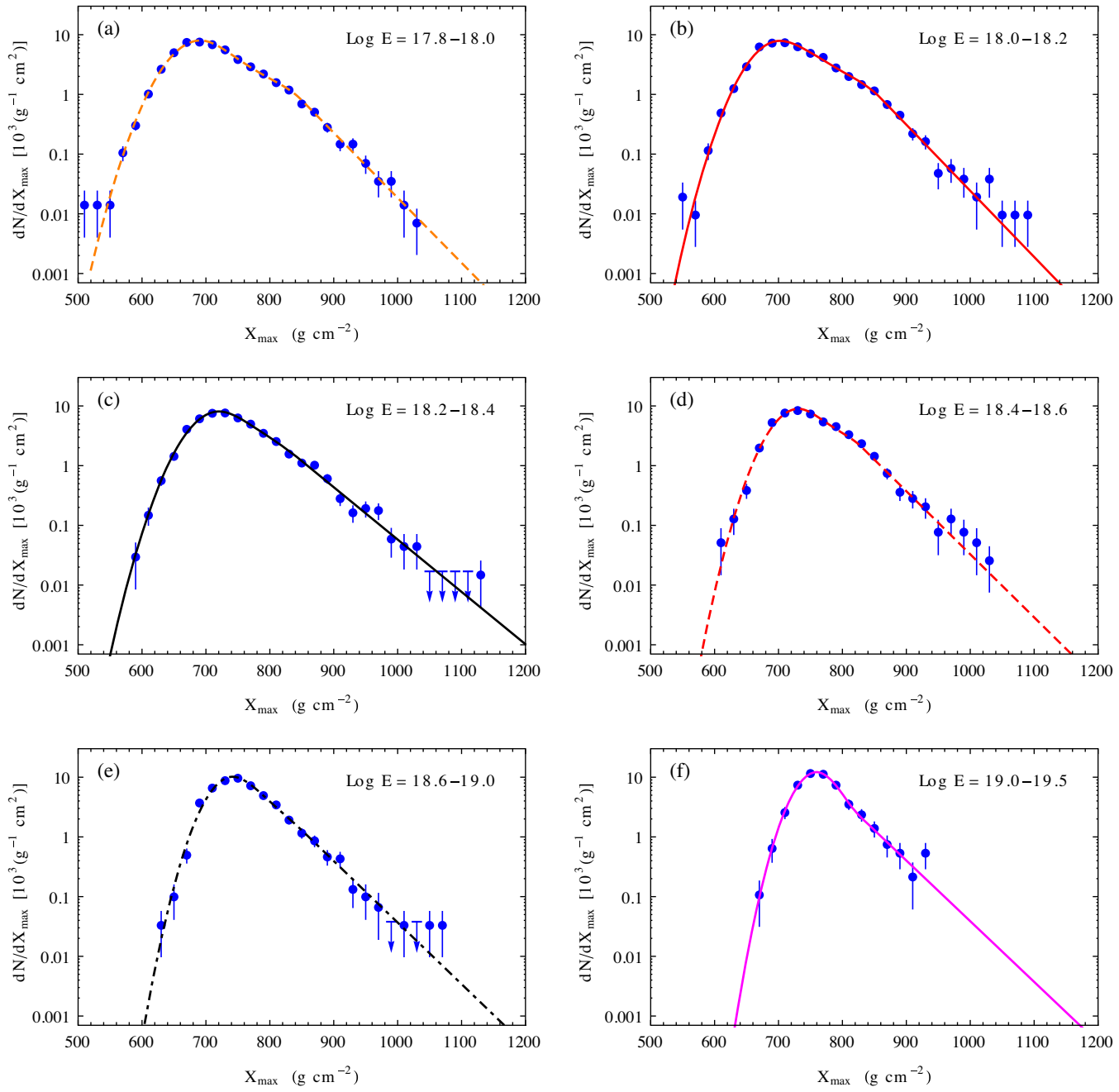

FIG. 17. Depth of maximum distributions of showers detected by Auger in different energy intervals [40,41]. The lines are fits discussed in the main text.

distribution from these data, for showers in the energy interval $10^{18.2}$–$10^{18.3}$ eV, has already been shown in Fig. 16, and compared with the distribution published in [14] where the showers were selected to have small detection acceptance distortions. The good agreement between these two datasets suggests that the detector acceptance effects are not very large.

Figure 17 shows (as histograms) the $X_{\rm max}$ distributions taken from [41] for six different energy intervals, together with fits (the lines) constructed joining three different functional forms in three $X_{\rm max}$ intervals:

(i) For $X_{\rm max} \leq X_{\rm peak}$ (with $X_{\rm peak}$ the position of the maximum of the distribution) the data is fitted with a Gaussian defined by three parameters: the position

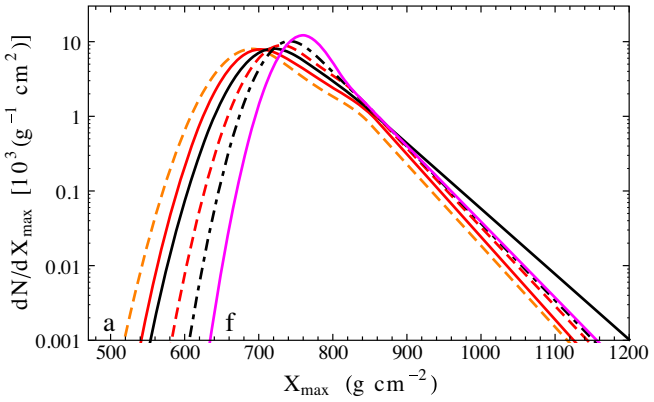

FIG. 18. Fits to the depth of maximum distributions of the CR showers detected by Auger [40,41] in six different energy intervals plotted together for comparison (all curves are normalized to unity). Comparisons of the fits with the data are shown in Fig. 17, the labeling of the curves (a, …, f) is the same as in the panels in that figure.

of the maximum $X_{\rm peak}$, the width $\sigma_{X,\rm left}$, and a normalization.

(ii) The tail of the distribution ($X_{\rm max} > X^*_{\rm max}$) is fitted with an exponential $F(X) = K^* e^{-X/\Lambda}$. The parameter $X^*_{\rm max}$ is determined from the data as the broadest range where an an exponential fit is of good quality. In the six energy intervals considered the best fit for $X^*_{\rm max}$ takes values between 830 and 860 g/cm^2. The quantities K^* and Λ, as discussed above, can be related to the p-air interaction length, and to the proton fraction.

(iii) The intermediate range ($X_{\rm peak} \le X \le X^*_{\rm max}$) is fitted with the form $F(X) = \exp[P(X)]$ where $P(X)$ a 3rd order polynomial in X. Three of the four parameters of the polynomial are, however, determined by the conditions that $F(X)$ is continuous at the two ends of the interval, and that the derivative $F'(X_{\rm peak}) = 0$.

This form provides a reasonably good quality fit to the data, and is in fact excellent for the Gaussian part (at small X) and for the exponential part (at large X). The six fits are shown together in Fig. 18, and the energy dependence of three parameters: $X_{\rm peak}$, $\sigma_{X,\rm left}$, and Λ is shown in Fig. 19.

The main goal of the presentation of this preliminary analysis is to illustrate the potential of a systematic study of the evolution with energy of the shape of the depth of maximum distribution. Not having included detector acceptance effects, it is not possible to reach firm conclusions, but it can be interesting to make a few remarks.

It is intriguing to note that (see the bottom panel of Fig. 19) the fitted value of the slope Λ on the energy interval between $10^{18.2}$ and $10^{18.4}$ eV, is consistent with the results published by Auger, while the values at both lower and higher energy are smaller, a result that can perhaps be attributed to a smaller proton fraction in the flux (or perhaps to detector biases).

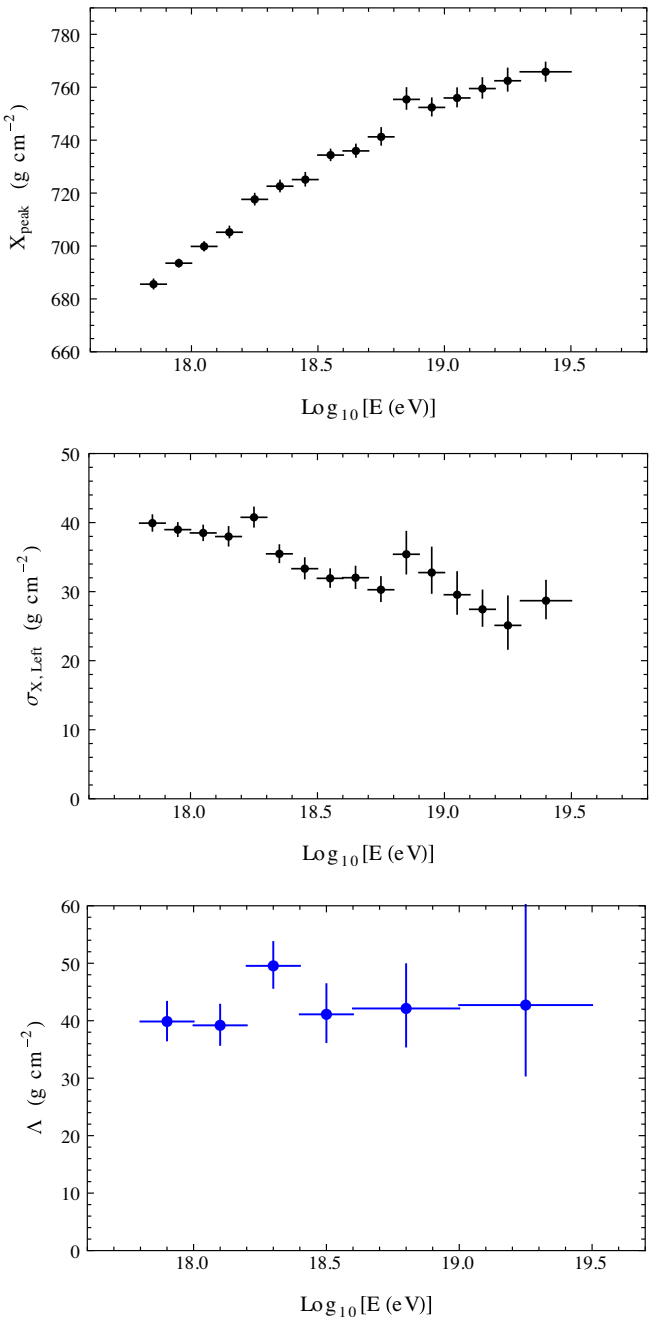

FIG. 19. Best fits parameters for the depth of maximum distributions of the Auger data (see Fig. 17). The top panel shows $X_{\rm peak}$, the value of X where the distribution has its maximum value. The middle panel shows $\sigma_{X,\rm left}$, the width of the Gaussian that fits the distribution for $X < X_{\rm peak}$. The bottom panel shows Λ, the slope of the tail of the distribution for large X values.

Also surprising is that the parameter $X^*_{\rm max}$, above which the distribution is well described by an exponential, is approximately constant, taking values from 830 to 860 g/cm^2 in the different energy intervals considered. The absolute normalizations of the distributions at

$X_{\max} \approx X^{*}_{\max}$ are also quite similar, an effect that can be clearly seen in Fig. 18 where all the fits (normalized to unity) are plotted together. Since the slopes of the distributions are also approximately constant, this also implies that the fraction of events in the exponential tail of the distribution changes only little with energy. For a pure proton composition the models predict distributions that have exponential tails that account for an approximately constant fraction of the events; however, the position of the tail covers an $X_{\max}$ that grows logarithmically with energy. In the absence of significant detection biases these results could be a hint for the presence of unexpected properties in shower development.

It can also be interesting to bring attention to the depth of maximum distribution for the highest energy interval (10^{19}–$10^{19.5}$ eV) shown in the last panel of Fig. 17, where there is a hint of a flattening at $X_{\max} \approx 800$ g/cm^2. As discussed above, for a pure proton composition the distribution must always have a slope larger than the asymptotic value [see Eq. (26)]. The flattening observed in the distribution for the highest energy showers can therefore be considered as a hint for a mixed composition, with a distribution dominated by a heavier (lighter) component below (above) the $X_{\max}$ of the flattening.

A more in depth study is clearly required to reach more firm conclusions. The phenomenological approach illustrated in this discussion should also be combined with the fitting of composition models using the methodology used in [5].

V. CONCLUSIONS AND OUTLOOK

Recent measurement of the energy spectrum and composition of UHECR have remarkable and very surprising implications for the properties of their astrophysical sources. The interpretation of the Auger measurements of the longitudinal development of the showers based on current models for hadronic interactions, indicates that the composition evolves with energy. Below the ankle (at $E \simeq 5 \times 10^{18}$ eV) the composition is consistent with a mixture of protons and intermediate mass nuclei, with the proton fraction increasing gradually. The result are consistent with a CR flux formed by two components of different spectral shape both of approximate power law form. Above the ankle the composition appears to change very rapidly, with nuclei of larger and larger mass becoming dominant as the energy increases. This can be interpreted with the hypothesis that the highest energy sources accelerate particles with a very hard spectrum up to a maximum rigidity that in good approximation is equal for all sources. The mass composition of the particles emitted by these sources is however quite unexpected. The implications of these results for high-energy astrophysics are profound, and constructing astrophysical models that reproduce these results is a very challenging task (see, for example, [35,42–50]).

It is obvious that it is very important to verify the Auger results with independent measurements [11,12], and to validate them with the ground array data [51]. It is however also very important to study critically how these results depend on the modeling of air shower development. The evolution of the CR composition emerge from the comparison of the data with models that describe hadronic interactions using extrapolations of the results obtained in accelerator experiments at lower energy, and therefore the possibility that the current models are incorrect, and that the interpretations based on them are not valid cannot at the moment be entirely excluded. It is therefore very desirable to develop methods that allow us to test this hypothesis. Combining the study of the CR composition with the measurement of the p-air cross section offers the possibility to perform very interesting studies.

Observations of the high-energy showers with the fluorescence technique allow to identify a proton component in the cosmic ray flux with a method that can be considered in good approximation as model independent. The point is that, for a fixed value of the energy, protons are the most penetrating component of the CR spectrum, and therefore (if they are present in the flux) will form the tail of the depth of maximum distribution for large values of $X_{\max}$. The shape of this tail, in good approximation, takes an exponential form with a slope that approaches the value of the p-air interaction length. The theoretical prediction based on extrapolations of accelerator experiments is a slope of order 50 g/cm^2 for $E \simeq 10^{18}$ eV, that changes only slowly with energy. The distributions for helium and more massive nuclei are predicted to have a shape that falls much more rapidly, (with a slope smaller that $\approx$30 g/cm^2). This difference allows to identify the presence of protons in the flux or the setting of an upper limit. This concept has been used to obtain measurements of the p-air interaction length for laboratory energies between 5×10^{17} and 5×10^{18} eV ($\sqrt{s} \approx 30$–95 TeV).

There are several reasons to combine the study of the CR composition (that is based of the global shape of the depth of maximum distributions) with the measurement of the p-air cross section (that is based on the shape of the distribution for the most penetrating showers). Such a combined approach, allows us to perform tests of the quality of the shower models, which must match the depth of maximum data in the exponential range (and therefore have the correct p-air cross section), and also for lower $X_{\max}$ values where the distribution flattens. This can result in more precise measurements of the proton component, and in smaller systematic errors. On the other hand, a composition study can constrain the contamination of helium (and more massive nuclei) in the spectrum, that in many cases is the dominant effect for the systematic error in the determination of proton cross section.

It is also very desirable to perform the combined study of CR composition and proton-air cross section systematically at all energies where data is available, even when the σ measurement has a very large error (or is not possible), because also in this case one can obtain valuable constraints on the CR composition. At the moment, for example, the highest measurements of the p-air cross section have been obtained by Telescope Array [15,16] at energies where the Auger Collaboration finds that the proton component is already significantly suppressed, and similarly only the Fly's Eye detector [13] has measured the p-air cross section at $E \simeq 10^{17.5}$ eV, an energy where the Auger results indicate that protons account for a fraction of order 50% of the total flux. The comparison of cross section measurements performed by different experiments at the same energies can be a useful method to test for the presence of systematic errors, and to reduce uncertainties on both the cross section values and the CR composition.

In this work we have limited our discussion to the study of fluorescence light observations, but very valuable information about the CR composition and about hadronic interactions are of course also encoded in the ground array data. A natural and very important goal for future studies is, however, to combine all the data, to study simultaneously the spectrum and composition of the primary flux and the properties of hadronic interactions that determine the properties of their showers. The results on the proton cross section and the proton fraction obtained from the interpretation of the depth of maximum distribution should then be studied together with the ground array data to improve our understanding of both particle physics and the high-energy universe.

ACKNOWLEDGMENTS

The first draft of this paper was prepared during a visit to the Auger site in occasion of the symposium for the 20th anniversary of the experiment. I am very grateful to the organizers for the kind invitation. I also acknowledge discussions withn Andrea Addazi, Xavier Bertou, Jose Bellido, Antonella Castellina, Armando Di Matteo, Ralph Engel, Tom Gaisser, Lorenzo Perrone, Viviana Scherini. Michael Unger, and Silvia Vernetto.

[1] A. Letessier-Selvon and T. Stanev, Ultrahigh energy cosmic rays, Rev. Mod. Phys. **83**, 907 (2011).
[2] A. Addazi *et al.*, Self-consistent approach for measuring the energy spectra and composition of cosmic rays and determining the properties of hadronic interactions at high energy, arXiv:2009.00851.
[3] J. Abraham *et al.* (Pierre Auger Collaboration), Observation of the Suppression of the Flux of Cosmic Rays above 4×10^{19} eV, Phys. Rev. Lett. **101**, 061101 (2008).
[4] T. Abu-Zayyad *et al.* (Telescope Array Collaboration), The cosmic ray energy spectrum observed with the surface detector of the telescope array experiment, Astrophys. J. Lett. **768**, L1 (2013).
[5] A. Aab *et al.* (Pierre Auger Collaboration), Depth of maximum of air-shower profiles at the Pierre Auger Observatory. II. Composition implications, Phys. Rev. D **90**, 122006 (2014).
[6] A. Aab *et al.* (Pierre Auger Collaboration), Combined fit of spectrum and composition data as measured by the Pierre Auger Observatory, J. Cosmol. Astropart. Phys. 04 (2017) 038; 03 (2018) 02(E).
[7] A. Castellina (Pierre Auger Collaboration), Highlights from the Pierre Auger Observatory (ICRC2019), Proc. Sci., ICRC2019 (**2020**) 004 [arXiv:1909.10791].
[8] A. Aab *et al.* (Pierre Auger Collaboration), Features of the Energy Spectrum of Cosmic Rays above 2.5×10^{18} eV Using the Pierre Auger Observatory, Phys. Rev. Lett. **125**, 121106 (2020).
[9] W. Hanlon, Telescope array 10 year composition, Proc. Sci., ICRC2019 (**2020**) 280 [arXiv:1908.01356].
[10] D. Bergman (Telescope Array Collaboration), Combined fit of the spectrum and composition from Telescope Array, Proc. Sci., ICRC2019 (**2020**) 190.
[11] M. Unger (Telescope Array Collaboration), Report of the working group on the composition of ultra-high energy cosmic rays, Proc. Sci., ICRC2015 (**2016**) 307.
[12] A. Yushkov *et al.* (Pierre Auger and Telescope Array Collaboration), Depth of maximum of air-shower profiles: Testing the compatibility of measurements performed at the Pierre Auger Observatory and the Telescope Array experiment, EPJ Web Conf. **210**, 01009 (2019).
[13] R. M. Baltrusaitis, G. L. Cassiday, J. W. Elbert, P. R. Gerhardy, S. Ko, E. C. Loh, Y. Mizumoto, P. Sokolsky, and D. Steck, Total Proton Proton Cross-Section at $\sqrt{s} = 30$-TeV, Phys. Rev. Lett. **52**, 1380 (1984).
[14] P. Abreu *et al.* (Pierre Auger Collaboration), Measurement of the Proton-Air Cross-Section at $\sqrt{s} = 57$ TeV with the Pierre Auger Observatory, Phys. Rev. Lett. **109**, 062002 (2012).
[15] R. U. Abbasi *et al.* (Telescope Array Collaboration), Measurement of the proton-air cross section with Telescope Arrays Middle Drum detector and surface array in hybrid mode, Phys. Rev. D **92**, 032007 (2015).
[16] R. U. Abbasi *et al.*, Measurement of the proton-air cross section with Telescope Array's black rock mesa and long ridge fluorescence detectors, and surface

array in hybrid mode, Phys. Rev. D **102**, 062004 (2020).
[17] R. Ulrich (Pierre Auger Collaboration), Extension of the measurement of the proton-air cross section with the Pierre Auger Observatory, Proc. Sci., ICRC2015 (**2016**) 401.
[18] R. J. Glauber and G. Matthiae, High-energy scattering of protons by nuclei, Nucl. Phys. **B21**, 135 (1970).
[19] A. Aab *et al.* (Pierre Auger Collaboration), A measurement of the cosmic-ray energy spectrum above 2.5×10^{18} eV using the Pierre Auger Observatory, Phys. Rev. D **102**, 062005 (2020).
[20] V. Verzi (Pierre Auger Collaboration), Measurement of the energy spectrum of ultra-high energy cosmic rays using the Pierre Auger Observatory, Proc. Sci. ICRC2019 (**2020**) 450.
[21] D. Ivanov (Telescope Array Collaboration), Energy spectrum measured by the Telescope Array, Proc. Sci. ICRC2019 (**2020**) 298.
[22] R. U. Abbasi *et al.* (Telescope Array Collaboration), The cosmic-ray energy spectrum between 2 PeV and 2 EeV observed with the TALE detector in monocular mode, Astrophys. J. **865**, 74 (2018).
[23] P. Lipari, Universality in the longitudinal development of cosmic ray showers, Nucl. Part. Phys. Proc. **279–281**, 111 (2016).
[24] K. H. Kampert and M. Unger, Measurements of the cosmic ray composition with air shower experiments, Astropart. Phys. **35**, 660 (2012).
[25] A. Yushkov (Pierre Auger Collaboration), Mass composition of cosmic rays with energies above $10^{17.2}$ eV from the hybrid data of the Pierre Auger Observatory, Proc. Sci. ICRC2019 (**2020**) 482.
[26] S. Ostapchenko, QGSJET-II: Physics, recent improvements, and results for air showers, EPJ Web Conf. **52**, 02001 (2013).
[27] T. Pierog, I. Karpenko, J. M. Katzy, E. Yatsenko, and K. Werner, EPOS LHC: Test of collective hadronization with data measured at the CERN large hadron collider, Phys. Rev. C **92**, 034906 (2015).
[28] A. Fedynitch, F. Riehn, R. Engel, T. K. Gaisser, and T. Stanev, Hadronic interaction model sibyll 2.3c and inclusive lepton fluxes, Phys. Rev. D **100**, 103018 (2019).
[29] R. U. Abbasi *et al.* (Telescope Array Collaboration), Depth of ultra high energy cosmic ray induced air shower maxima measured by the telescope array black rock and long ridge FADC fluorescence detectors and surface array in hybrid mode, Astrophys. J. **858**, 76 (2018).
[30] A. Aab *et al.* (Pierre Auger Collaboration), Evidence for a mixed mass composition at the 'ankle' in the cosmic-ray spectrum, Phys. Lett. B **762**, 288 (2016).
[31] A. Aab *et al.* (Pierre Auger Collaboration), Inferences on mass composition and tests of hadronic interactions from 0.3 to 100 EeV using the water-Cherenkov detectors of the Pierre Auger Observatory, Phys. Rev. D **96**, 122003 (2017).
[32] A. Aab *et al.* (Pierre Auger Collaboration), Testing Hadronic Interactions at Ultrahigh Energies with Air Showers Measured by the Pierre Auger Observatory, Phys. Rev. Lett. **117**, 192001 (2016).
[33] R. U. Abbasi *et al.* (Telescope Array Collaboration), Study of muons from ultrahigh energy cosmic ray air showers measured with the Telescope Array experiment, Phys. Rev. D **98**, 022002 (2018).
[34] L. Cazon *et al.* Working group report on the combined analysis of muon density measurements from eight air shower experiments, Proc. Sci., ICRC2019 (**2020**) 214 [arXiv:2001.07508].
[35] M. Unger, G. R. Farrar, and L. A. Anchordoqui, Origin of the ankle in the ultrahigh energy cosmic ray spectrum, and of the extragalactic protons below it, Phys. Rev. D **92**, 123001 (2015).
[36] E. J. Ahn, R. Engel, T. K. Gaisser, P. Lipari, and T. Stanev, Cosmic ray interaction event generator SIBYLL 2.1, Phys. Rev. D **80**, 094003 (2009).
[37] G. Antchev *et al.* (TOTEM Collaboration), Luminosity-independent measurements of total, elastic and inelastic cross-sections at $\sqrt{s} = 7$ TeV, Europhys. Lett. **101**, 21004 (2013).
[38] G. Antchev *et al.* (TOTEM Collaboration), Luminosity-Independent Measurement of the Proton-Proton Total Cross Section at $\sqrt{s} = 8$ TeV, Phys. Rev. Lett. **111**, 012001 (2013).
[39] G. Antchev *et al.* (TOTEM Collaboration), First measurement of elastic, inelastic and total cross-section at $\sqrt{s} =$ 13 TeV by TOTEM and overview of cross-section data at LHC energies, Eur. Phys. J. C **79**, 103 (2019).
[40] A. Aab *et al.* (Pierre Auger Collaboration), Depth of maximum of air-shower profiles at the Pierre Auger Observatory: Measurements at energies above $10^{17.8}$ eV, Phys. Rev. D **90**, 122005 (2014).
[41] https://www.auger.org/index.php/science/data.
[42] R. Aloisio, V. Berezinsky, and P. Blasi, Ultra high energy cosmic rays: Implications of Auger data for source spectra and chemical composition, J. Cosmol. Astropart. Phys. 10 (2014) 020.
[43] N. Globus, D. Allard, and E. Parizot, A complete model of the cosmic ray spectrum and composition across the Galactic to extragalactic transition, Phys. Rev. D **92**, 021302 (2015).
[44] A. M. Taylor, M. Ahlers, and D. Hooper, Indications of negative evolution for the sources of the highest energy cosmic rays, Phys. Rev. D **92**, 063011 (2015).
[45] S. Thoudam, J. P. Rachen, A. van Vliet, A. Achterberg, S. Buitink, H. Falcke, and J. R. Hörandel, Cosmic-ray energy spectrum and composition up to the ankle: The case for a second Galactic component, Astron. Astrophys. **595**, A33 (2016).
[46] A. Yushkov, M. Risse, M. Werner, and J. Krieg, Determination of the proton-to-helium ratio in cosmic rays at ultra-high energies from the tail of the $X_{\max}$ distribution, Astropart. Phys. **85**, 29 (2016).
[47] I. I. Karpikov, G. I. Rubtsov, and Y. V. Zhezher, Lower limit on the ultrahigh-energy proton-to-helium ratio from the measurements of the tail of the $X_{\max}$ distribution, Phys. Rev. D **98**, 103002 (2018).
[48] P. Mészáros, D. B. Fox, C. Hanna, and K. Murase, Multi-messenger astrophysics, Nat. Rev. Phys. **1**, 585 (2019).

[49] S. Mollerach and E. Roulet, Extragalactic cosmic rays diffusing from two populations of sources, Phys. Rev. D **101**, 103024 (2020).

[50] S. Das, S. Razzaque, and N. Gupta, Modeling the spectrum and composition of ultrahigh-energy cosmic rays with two populations of extragalactic sources, Eur. Phys. J. C **81**, 59 (2021).

[51] A. Aab *et al.* (Pierre Auger Collaboration), The Pierre Auger Observatory upgrade—Preliminary design report, arXiv: 1604.03637.